

# Black holes and asymptotically safe gravity

Kevin Falls, Daniel F. Litim, and Aarti Raghuraman

*Department of Physics and Astronomy, University of Sussex, Brighton BN1 9QH, U.K.*

Quantum gravitational corrections to black holes are studied in four and higher dimensions using a renormalisation group improvement of the metric. The quantum effects are worked out in detail for asymptotically safe gravity, where the short distance physics is characterized by a non-trivial fixed point of the gravitational coupling. We find that a weakening of gravity implies a decrease of the event horizon, and the existence of a Planck-size black hole remnant with vanishing temperature and vanishing heat capacity. The absence of curvature singularities is generic and discussed together with the conformal structure and the Penrose diagram of asymptotically safe black holes. The production cross section of mini-black holes in energetic particle collisions, such as those at the Large Hadron Collider, is analysed within low-scale quantum gravity models. Quantum gravity corrections imply that cross sections display a threshold, are suppressed in the Planckian, and reproduce the semi-classical result in the deep trans-Planckian region. Further implications are discussed.

## I. INTRODUCTION

Black holes are intriguing solutions to Einstein's classical equations for gravity, characterized by conserved global charges such as total mass, angular momentum, or electric charge. Most prominently black holes display an event horizon which classically cannot be crossed by light rays emitted from their interior. The simplest black hole solution in four dimensions, the Schwarzschild black hole, has been discovered nearly a century ago [1], and many more solutions with increasing degree of complexity are known by now both in lower and in higher dimensions. The latter have received much attention recently due to qualitatively new solutions such as black rings which cannot be realised in a low dimensional setup [2].

Recently, the physics of higher dimensional black holes has become of particular interest for the phenomenology of particle physics at colliders. In models where gravity propagates in a higher-dimensional space time while Standard Model particles are constraint to a four-dimensional brane [3, 4], the fundamental quantum gravity scale is as low as the electroweak scale. This opens the exciting possibility that particle colliders such as the LHC could become the first experiment to provide evidence for the quantisation of gravity. Signatures of low-scale quantum gravity from particle collisions include real and virtual graviton effects [5], and the production and decay of TeV size black holes [6, 7].

It is widely expected that a semi-classical description of black hole production and decay is applicable provided curvature effects remain small, and as long as the black hole mass is large compared to the Planck scale [8, 9]. Then the fundamental black hole production cross section is estimated by the geometric one, modulo grey body factors reflecting impact parameter dependences and inefficiencies in the formation of a horizon [10].

The inclusion of quantum gravitational corrections to the dynamics of space-time becomes a challenge once

the black hole mass approaches the fundamental Planck scale. Here, quantum gravity effects are central for black hole production, decay, or the final stages of a gravitational collapse. Furthermore, the quantisation of matter fields on a black hole background and the very notion of a black hole temperature has to be revisited once quantum fluctuations of space-time itself become dominant. An understanding of the Planckian regime should clarify the so-called 'information paradox' and the ultimate fate of an evaporating black hole.

Presently, a complete quantum gravity description of the above phenomena is not at hand. Furthermore, the standard perturbative quantisation for gravity still faces problems. Important advances, however, have been achieved along the lines of Steven Weinberg's asymptotic safety scenario [11]. This set-up circumvents the virulent divergences encountered within perturbation theory and leads to well-defined physical observables, such as  $S$ -matrix elements, provided that gravity displays a non-trivial high-energy fixed point under the renormalisation group [12–16]. This intriguing picture implies a non-perturbative ultraviolet completion for gravity, where the metric fields remain the fundamental degrees of freedom. Most importantly, the low energy regime of classical general relativity is linked with the high energy regime by a well-defined, finite, renormalisation group trajectory [16].

In this paper, we study quantum corrections to black holes in higher dimensions in the context of asymptotically safe gravity, the main results of which have been summarized in [17, 18]. It is our central assumption that the leading quantum gravity corrections to black hole metrics are accounted for by replacing Newton's coupling constant through a 'running' coupling which evolves under the renormalisation group equations for gravity. Our approach is informed by recent RG results for higher dimensional quantum gravity [12, 16, 19–21], and by earlier black hole studies in the four-dimensional case [22–24]. Our findings are relevant for the phenomenology

of e.g. mini-black hole production at colliders. Further signatures of asymptotically safe quantum gravity at colliders have been analysed in [25–27].

The paper is organized as follows. We first recall the essentials of classical black holes, and outline the qualitative picture (Sec. II). This is followed by a discussion of the renormalisation group equations for the running of Newton’s coupling within asymptotically safe gravity (Sec. III). We construct improved black holes in four and higher dimensions, and analyse their main characteristics including the horizon structure, mass dependence, the existence of smallest black holes (Sec. IV), as well as their singularity and causality structure (Sec. V). Our findings are applied to the physics of black hole production in higher dimensional scenarios with low-scale quantum gravity (Sec. VI). We close with a discussion of the main results and indicate further implications (Sec. VII).

## II. GENERALITIES

In this section, we recall the basics of classical black holes, introduce some notation, outline the renormalisation group improvement for black hole metrics and discuss first implications.

### A. Schwarzschild metric

The classical, static, spherically symmetric, non-charged black hole solution to Einstein’s equation is the well-known Schwarzschild black hole [1]. Its line element in  $d \geq 4$  dimensions is given by [28] (see also [29])

$$ds^2 = -f(r) dt^2 + \frac{dr^2}{f(r)} + r^2 d\Omega_{d-2}^2. \quad (2.1)$$

The lapse function

$$f(r) = 1 - \frac{G_N M}{r^{d-3}} \quad (2.2)$$

depends on Newton’s coupling constant  $G_N$  in  $d$  dimensions. The reduced black hole mass  $M$  is

$$M = \frac{8 \Gamma(\frac{d-1}{2})}{(d-2)\pi^{(d-3)/2}} M_{\text{phys}}, \quad (2.3)$$

with  $M_{\text{phys}}$  the physical mass of the black hole. In terms of these, the classical Schwarzschild radius  $r_{\text{cl}}$  is given as

$$r_{\text{cl}}^{d-3} = G_N M. \quad (2.4)$$

The black hole solution is continuous in the mass parameter  $M$  and displays a Bekenstein-Hawking temperature inversely proportional to its mass. For large radial distance  $r \rightarrow \infty$ , we observe  $f(r) \rightarrow 1$ , indicating

that the geometry of a Schwarzschild space-time becomes flat Minkowskian. The coordinate singularity at  $r = r_{\text{cl}}$  where  $f(r_{\text{cl}})$  vanishes, defines the event horizon of the black hole. In the short distance limit  $r \rightarrow 0$  we observe a divergence in  $f(r)$ , reflecting a metric and curvature singularity at the origin.

### B. Improved metric

The classical black hole is modified once quantum gravitational effects are taken into account. In general, quantum fluctuations will modify the gravitational force law by turning Newton’s coupling  $G_N$  into a distance-dependent “running” coupling  $G(r)$ ,

$$G_N \rightarrow G(r). \quad (2.5)$$

It is the central assumption of this paper that the leading quantum gravitational corrections to the black hole are captured by the replacement (2.5) in the metric (2.2). This “renormalisation group improvement” should provide a good description of the leading quantum corrections, because the primary, explicit, dependence of the Schwarzschild black hole on the gravitational sector is only via Newton’s coupling  $G_N$ . Furthermore, the classical black hole solution is continuous in its mass parameter  $M$ , and the effects of quantum corrections are parametrically suppressed for large black hole mass with  $M_D/M$  serving as an external, small, control parameter. Whether gravity becomes “strong” at shortest distances, or “weak”, will depend on the ultraviolet completion for gravity and the related running under the renormalisation group.

Next we discuss the main implications arising from a running gravitational coupling. For the sake of the argument, we parametrize  $G(r)$  as

$$G(r) = r_{\text{char}}^{d-2} \left( \frac{r}{r_{\text{char}}} \right)^\alpha \quad (2.6)$$

for sufficiently small  $r$ , where  $r_{\text{char}}$  denotes a characteristic length scale where quantum corrections become dominant. The index  $\alpha$  then parametrizes the gravitational coupling strength at short distances, with  $\alpha > 0$  ( $\alpha < 0$ ) denoting a decrease (increase) of  $G(r)/G_N$  at small distances, respectively, and the classical limit  $\alpha = 0$  where  $r_{\text{char}}$  is given by the Planck length  $r_{\text{char}} = 1/M_D$ . The behaviour of  $f(r \rightarrow 0)$ , and the solutions to the horizon condition  $f(r) = 0$  then teach us how the RG-improved black hole depends on the quantum effects parametrized by  $\alpha$ . The qualitative pattern is summarised in Tab. 1. We distinguish three cases, depending on the short distance index  $\alpha$ :

case	short distance index	gravity	horizons	$f(r \rightarrow 0)$
(i)	$\alpha < d - 3$	strong, if $\alpha < 0$ ; weak, if $\alpha > 0$	one	singular
(ii)	$\alpha = d - 3$	weak	none, one or more	finite
(iii)	$\alpha > d - 3$	weak	none, one or more	1

Table 1: Horizons of quantum-corrected Schwarzschild black holes assuming a scale-dependent gravitational coupling strength (2.6) at short distances for various dimensions and in dependence on the short distance index  $\alpha$  (see text).

- (i)  $\alpha < d - 3$ . In this case the gravitational coupling either increases with decreasing  $r$ , or even decreases slightly, though not strongly enough to overcome the enhancement due to the  $\frac{1}{r^{d-3}}$ -factor in (2.2). Therefore  $f(r)$  unavoidably has to change sign leading to a horizon. This includes the classical case  $\alpha = 0$ , and all cases of strong gravity corresponding to a diverging  $G(r)/G_N$  for small  $r$ . Interestingly, even if gravity weakens at short distances with an index  $0 < \alpha < d - 3$ , we still observe a horizon for arbitrary small black hole masses.
- (ii)  $\alpha = d - 3$ . In this case, we have a finite limit  $f(r \rightarrow 0) = f_0$ . For  $f_0 < 0$ , this necessarily enforces a horizon, similar to case (i). For  $f_0 > 0$ , the situation is analogous to case (iii).
- (iii)  $\alpha > d - 3$ . In this case,  $G(r)$  weakens fast enough to overcome the enhancement due to  $\frac{1}{r^{d-3}}$ . Therefore  $f(r \rightarrow 0) \rightarrow 1$  and  $f(r)$  may display either several zeros, a single one, or none at all, leading to several, one or no horizon depending on the black hole mass  $M$  and the precise short-distance behaviour of  $G(r)$ .

We conclude that for  $\alpha > d - 3$  the Schwarzschild black hole may no longer display a horizon for all mass, whereas for  $\alpha < d - 3$  a horizon is guaranteed for all  $M$ . Which of these scenarios is realised depends on the short-distance behaviour of gravity. In the remaining part of the paper we access this picture quantitatively, using the renormalisation group for gravity.

### III. ASYMPTOTICALLY SAFE GRAVITY

In this section, we discuss field theory based approaches to quantum gravity including effective theory and the asymptotic safety scenario for gravity, and provide the renormalisation group running for Newton's coupling.

#### A. Effective theory for gravity

In the absence of a complete theory for quantum gravity, quantum corrections of the form (2.5) can be accessed in the weak gravity regime using methods from

effective theory [30, 31]. In practice, this amounts to an ultraviolet regularisation of the theory by an UV cutoff  $\Lambda$  of the order of the fundamental Planck scale. In the weak gravity regime where  $r M_D \gg 1$  with Planck mass  $M_D = (G_N)^{-1/(d-2)}$ , it has been found that

$$G(r) = G_N \left( 1 - \frac{\omega G_N}{r^2} \right) \quad (3.1)$$

in four dimensions, and at the one-loop order [32–35], with  $\omega > 0$  (see [36] for earlier results). In higher dimensions, no effective theory results are available and thus we have to provide the relevant RG input from a different source.

#### B. Asymptotic safety

Asymptotic safety of gravity is a scenario where gravity exists as a well-defined fundamental local quantum theory of the metric field [11]. This set-up goes one step beyond an effective theory approach: it assumes that the ultraviolet cutoff  $\Lambda$  from effective theory can safely be removed,  $\Lambda \rightarrow \infty$ , whereby the relevant gravitational couplings approach a non-trivial fixed point [12–16]. We briefly recall the main picture. Consider the dimensionless gravitational coupling

$$g(\mu) = G(\mu)\mu^{d-2} \equiv G_0 Z_G^{-1}(\mu)\mu^{d-2}, \quad (3.2)$$

where  $\mu$  denotes the RG momentum scale,  $G(\mu)$  is the running Newton coupling, and  $Z_G$  the gravitational wave function factor. The wave function factor is normalised as  $Z_G(\mu_0) = 1$  at some reference scale  $\mu_0$  with  $G(\mu_0)$  given by Newton's constant  $G_0 \equiv G_N$ . Then the gravitational Callan-Symanzik equation reads [13, 19]

$$\frac{dg(\mu)}{d \ln \mu} = (d - 2 + \eta)g(\mu). \quad (3.3)$$

Here  $\eta = -\mu \partial_\mu \ln Z_G$  denotes the anomalous dimension of the graviton. In general, the anomalous dimension depends on all couplings of the theory. Due to its structure, (3.3) can achieve two types of fixed points. At small coupling, the anomalous dimension vanishes and  $g = 0$  corresponds to the non-interacting (*i.e.* Gaussian) fixed point of (3.3). This fixed point dominates the deep infrared region of gravity  $\mu \rightarrow 0$ . In turn, an interacting

fixed point  $g_*$  is achieved if the anomalous dimension of the graviton becomes non-perturbatively large,

$$\eta_* = 2 - d. \quad (3.4)$$

A non-trivial fixed point of quantum gravity in  $d > 2$  implies a negative integer value for the graviton anomalous dimension, counter-balancing the canonical dimension of  $G$ . As a consequence,  $G(\mu) \rightarrow g_*/\mu^{d-2}$  in the vicinity of a non-trivial fixed point. In the UV limit where  $\mu \rightarrow \infty$ , the gravitational coupling  $G(\mu)$  becomes arbitrarily weak.

### C. Renormalisation group

The above picture is substantiated through explicit renormalisation group studies for gravity. A powerful tool is given by the functional renormalisation group [37], based on the idea of integrating-out momentum modes from a path-integral representation of quantum field theory [13, 14, 16]. The corresponding ‘flowing’ effective action for gravity reads

$$\Gamma_k = \frac{1}{16\pi G_k} \int d^d x \sqrt{g} [-R(g) + \dots]. \quad (3.5)$$

Here  $R(g)$  denotes the Ricci scalar, and the dots in (3.5) stand for the cosmological constant, higher dimensional operators in the metric field, gravity-matter interactions, a classical gauge fixing and ghost terms. Furthermore, all couplings in (3.5) are ‘running’ couplings as functions of the Wilsonian momentum scale  $k$ , which now takes over the role of the RG scale  $\mu$  discussed above. The action (3.5) reduces to the standard quantum effective action in the limit  $k \rightarrow 0$ , where all quantum fluctuations are integrated out. For  $k \ll M_D$ , the gravitational sector is well-approximated by the Einstein-Hilbert action with  $G_k \approx G_0$ , and similarly for the gravity-matter couplings. The corresponding operators scale canonically. At  $k \approx M_D$  and above, the non-trivial RG running of gravitational couplings becomes important.

An exact functional flow equation which governs the  $k$ -dependence for an action (3.5) has been put forward by Wetterich [38],

$$\partial_t \Gamma_k = \frac{1}{2} \text{Tr} \left( \Gamma_k^{(2)} + R_k \right)^{-1} \partial_t R_k \quad (3.6)$$

and  $t = \ln k$ . The trace stands for a momentum integration and a sum over indices and fields, and  $R_k(q^2)$  denotes an appropriate infrared cutoff function at momentum scale  $q^2 \approx k^2$  [39]. The flow (3.6) can be seen as a functional Callan-Symanzik equation, where the mass term is replaced by a momentum-dependent mass  $k^2 \rightarrow R_k(q^2)$  [40]. When implemented for gravity [41], an additional background field is introduced to achieve diffeomorphism

invariance within the background field technique [37, 41–43]. By now, a large number of papers have shown the existence of a non-trivial fixed point for gravity including renormalisation group studies in four and higher dimensions [19–21, 41, 44–57], and numerical simulations on the lattice [58, 59].

Analytical results for the running of the gravitational coupling have been given in [19], where (3.5) has been approximated by the Ricci scalar. The central result is not altered through the inclusion of a cosmological constant [20]. Using (3.5) and (3.6), one finds

$$\beta_g = \frac{(1 - 4dg/c_d)(d-2)g}{1 - (2d-4)g/c_d} \quad (3.7)$$

with parameter  $c_d = (4\pi)^{d/2-1} \Gamma(\frac{d}{2} + 2)$ . The scale-dependence of the anomalous dimension is given via the scale-dependence of the running coupling,

$$\eta = \frac{2(d-2)(d+2)g/c_d}{2(d-2)g/c_d - 1}. \quad (3.8)$$

We observe a Gaussian fixed point at  $g_* = 0$  and a non-Gaussian one at  $g_* = c_d/(4d)$ . Integrating the flow (3.7) gives an implicit equation for  $G_k$ ,

$$\frac{G(k)}{G(k_0)} = \left( \frac{g_* - G(k)k^{d-2}}{g_* - G(k_0)k_0^{d-2}} \right)^{(d-2)/\theta} \quad (3.9)$$

with boundary condition  $G(k_0)k_0^{d-2} < g_*$ , and the non-perturbative scaling exponent  $\theta = 2d \frac{d-2}{d+2}$ . The fixed point value and the scaling exponent depend slightly on the underlying momentum cutoff [19, 20]. Inserting the running coupling (3.9) into (3.7) shows that the anomalous dimension displays a smooth cross-over between the IR domain  $k \ll M_D$  where  $\eta \approx 0$  and the UV domain  $k \gg M_D$  where  $\eta \approx 2-d$ . The cross-over regime becomes narrower with increasing dimension. For our purposes, it will be sufficient to approximate the non-perturbative solution (3.9) further by setting the scaling index  $\theta$  to  $\theta = d-2$ . In the limit where  $G(k_0)k_0^{d-2} \ll 1$ , we find

$$\frac{1}{G(k)} = \frac{1}{G_0} + \omega k^{d-2} \quad (3.10)$$

where  $\omega = 1/g_*$  is a positive constant, and  $G_0 = G(k_0 = 0)$ . Note that (3.10) looks, formally, like a 1-loop equation. The difference here is that the coefficient  $\omega$ , in general, also encodes information about the underlying fixed point and may be numerically different from the 1-loop coefficient. This equation captures the main cross-over behaviour.

### D. Relevant scales

In order to implement quantum corrections to the classical Schwarzschild black hole geometry, we replace the

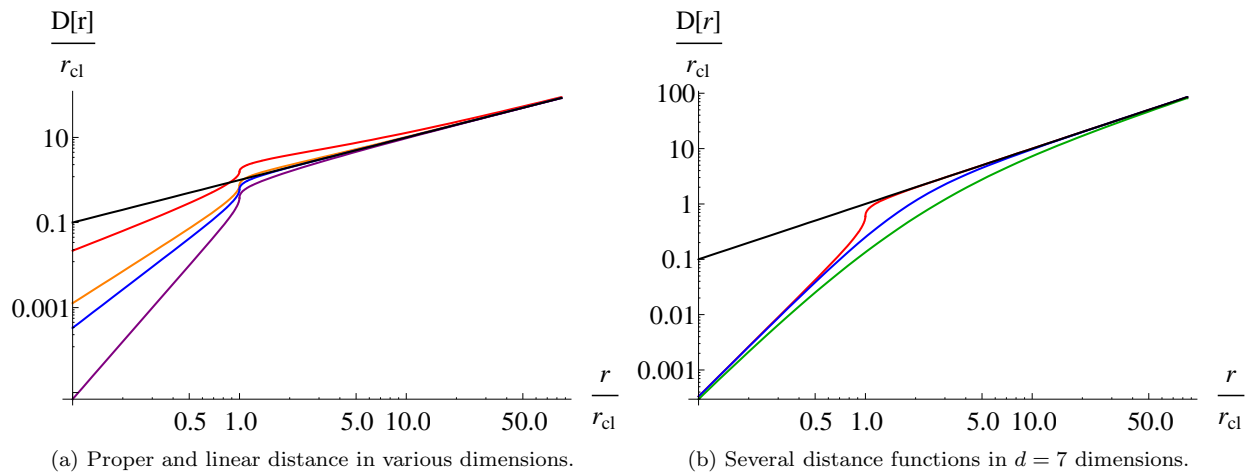


Figure 1: Comparison of various distance functions  $D(r)$  as functions of  $r/r_{\text{cl}}$ . (a) Proper distance in  $d = 4, 6, 7$  and  $10$  dimensions (top to bottom) and linear matching (straight line). (b) Interpolating expressions (3.19) and (3.21), proper distance matching (3.16), and linear matching (3.17) (bottom to top) in 7 dimension.

classical coupling  $G$  by an  $r$ -dependent running coupling  $G(r)$  under the RG flow. The renormalisation group provides us with a momentum-scale dependent  $G(k)$ . This requires, additionally, a scale identification between the momentum scale  $k$  and the coordinate variable  $r$  of the form

$$k(r) = \xi/D(r), \quad (3.11)$$

such that

$$\frac{1}{G(r)} = \frac{1}{G_0} + \frac{\omega \xi^{d-2}}{D^{d-2}(r)}. \quad (3.12)$$

The distance function  $D(r)$  should be an appropriately chosen length scale which may depend on other parameters such as eg. the black hole mass  $M$ . In general, the matching coefficient  $\xi$  is non-universal and its numerical value will depend on the RG scheme used to obtain the RG running of  $G(k)$ . In a fixed RG scheme, and for a given choice for  $D(r)$ ,  $\xi$  can be computed explicitly using methods discussed in eg. [30].

Next we introduce a variety of distance functions motivated by the Schwarzschild metric, flat space metric, dimensional analysis, and interpolations.

• *Dimensional analysis.* The gravitational force on a test particle in a Schwarzschild space-time depends on two independent dimensionful parameters, the horizon  $r_{\text{cl}}$  (or the black hole mass, respectively) and the radial distance scale  $r$ . Therefore, dimensional analysis suggests that a general length scale  $D(r)$  can be written as

$$D_{\text{da}}(r) = c_\gamma r^\gamma r_{\text{cl}}^{-\gamma+1}. \quad (3.13)$$

for some  $\gamma$ , and  $c_\gamma$  a positive constant. Moreover,  $\gamma$  may depend on dimensionless ratios such as  $r/r_{\text{cl}}$ . An ansatz

taking into account the flat-space limit for  $r \rightarrow \infty$ , and the deep Schwarzschild regime  $r \ll r_{\text{cl}}$ , is given by

$$D_{\text{da}}(r) \propto \begin{cases} r & \text{for } r > r_{\text{cl}} \\ r^\gamma r_{\text{cl}}^{-\gamma+1} & \text{for } r < r_{\text{cl}} \end{cases} \quad (3.14)$$

with coefficient  $\gamma$ . In the parametrisation (2.6), this corresponds to the short-distance index  $\alpha = \gamma(d-2)$ . For  $\gamma > 1$  ( $\gamma < 1$ ), the matching enhances (counteracts) the RG running of (3.10). We note that  $1/\gamma \rightarrow 0$  corresponds to a decoupling limit where gravity is switched-off at scales below  $r_{\text{cl}}$ .

• *Proper distance.* A different matching is obtained by identifying the RG momentum scale  $k$  with the inverse diffeomorphism invariant distance  $D_{\text{diff}}(r)^{-1}$  [22]. Such a distance is defined through the line integral

$$D_{\text{diff}}(r) = \int_C \sqrt{|ds^2|}, \quad (3.15)$$

where  $C$  is an appropriately chosen curve in spacetime. Using the classical Schwarzschild metric, we consider a path  $C$  running radially from 0 to  $r$ , thereby connecting time-like with space-like regions. With  $dt = d\Omega = 0$  this defines the proper distance

$$D_{\text{Schw}}(r) = \int_0^r dr \left| 1 - \left( \frac{r_{\text{cl}}}{r} \right)^{d-3} \right|^{-1/2}. \quad (3.16)$$

For any  $d$ , (3.16) has an integrable pole  $\sim 1/\sqrt{r-r_{\text{cl}}}$  at the connection point between space-like and time-like regions  $r = r_{\text{cl}}$ . Analytical expressions for  $D_{\text{Schw}}(r)$  are obtained from (3.16) for fixed dimension. We note that (3.16) corresponds to (3.13) with an  $(r/r_{\text{cl}})$ -dependent index  $\gamma$ . For large  $r \gg r_{\text{cl}}$ , we have  $D_{\text{Schw}}(r) \rightarrow r$ , where the Schwarzschild metric becomes flat corresponding to

$\gamma = 1$  in (3.13). For small  $r$  (3.16) corresponds to (3.13) with  $\gamma = (d-1)/2$ .

- *IR matching.* If the black hole mass  $M$  is sufficiently large compared to the Planck mass, we can assume that the only RG relevant length scale in the problem is given by  $r$ . Therefore,  $r$  is directly identified with the (inverse) RG scale  $k$ ,

$$D_{\text{ir}}(r) = r. \quad (3.17)$$

This matching (3.17) corresponds to (3.13) with  $\gamma = c_\gamma = 1$ . In the parametrisation (2.6), the short distance behaviour corresponds to  $\alpha = d-2$ . We therefore expect the matching (3.17) to capture the leading quantum effects correctly.

- *UV matching.* For small  $r \ll r_{\text{cl}}$ , the proper distance  $D_{\text{Schw}}(r)$  scales like a power-law in  $r$ . We find

$$D_{\text{uv}}(r) = \frac{2 r^{(d-1)/2}}{(d-1) r_{\text{cl}}^{(d-3)/2}}. \quad (3.18)$$

Matching the RG momentum scale with the inverse proper distance (3.18) leads to (3.13) with  $\gamma = c_\gamma^{-1} = (d-1)/2$ . In the parametrisation (2.6), this corresponds to the short-distance index  $\alpha = (d-1)(d-2)/2 > 0$ , which for all  $d > 3$  is larger than the index  $(d-2)$  obtained from linear matching.

- *Interpolations.* For the subsequent analysis, it is useful to have approximate expressions for  $D_{\text{Schw}}(r)$  (3.16) which interpolate properly between (3.17) and (3.18). We use a simple interpolation formula for general dimension to implement the non-linear matching (3.16) into (3.10) and write

$$D_{\text{int1}}(r) = \frac{2 r^{(d-1)/2}}{(d-1) (r_{\text{cl}} + \epsilon r)^{(d-3)/2}} \quad (3.19)$$

$$\epsilon = \left(\frac{d}{2} - \frac{1}{2}\right)^{-2/(d-3)} \quad (3.20)$$

which is exact for  $r \rightarrow \infty$  and  $r \rightarrow 0$ , and  $\epsilon \in [\frac{4}{9}, 1]$  for  $d \in [4, \infty]$ . Alternatively, we also use

$$D_{\text{int2}}(r) = \frac{r}{1 + \frac{1}{2}(d-1) (r_{\text{cl}}/r)^{(d-3)/2}}. \quad (3.21)$$

In Fig. 1 we compare different distance functions. In Fig. 1(a), the functions (3.16) are compared with the linear matching (3.17) in various dimensions. For large  $r$  the proper distance (3.16) approaches  $r$  for all  $d \geq 4$ . As  $r/r_{\text{cl}} \searrow 1$  we observe that the gradient steepens rapidly due to the presence of an integrable pole  $1/\sqrt{r-r_{\text{cl}}}$ . For  $r \ll r_{\text{cl}}$  the gradients of each curve are steeper with increasing  $d$  due to an additional dimensional suppression in (3.16). In Fig. 1(b) we fix  $d = 7$  and observe that for large  $r$  the matchings (3.16), (3.19) and (3.21) approach the correct IR behaviour (3.17). For small  $r$  these matchings approach the UV matching (3.18). We also observe

that the rapid steepening of (3.16) around  $r/r_{\text{cl}}$  implies that the transition between IR and UV behaviour is well approximated by (3.14).

Finally, we provide a link with the discussion of Tab. 1, see Sec. II B. For the distance functions motivated by the Schwarzschild metric (3.16), (3.18), (3.19) and (3.21), we find the index  $\alpha = \frac{1}{2}(d-1)(d-2) > (d-3)$  for all  $d \geq 4$ , corresponding to case (iii). In the same vein, for  $D(r)$  motivated by the flat space metric (3.17) we find  $\alpha = d-2$  equally corresponding to case (iii). Finally, the distance function motivated by dimensional analysis (3.14) contains a free parameter  $\gamma$ , whose natural value is of order one. It leads to the index  $\alpha = \gamma(d-2)$  and hence relates to case (iii) for all  $\gamma > \gamma_c$ , where

$$\gamma_c = \frac{d-3}{d-2}. \quad (3.22)$$

We conclude that for all physically motivated distance functions we are lead to the scenario described by case (iii) in Tab. 1, independently of the scale identification  $k = k(r)$ . This, therefore, appears to be a robust prediction from the renormalisation group running implied within asymptotically safe gravity.

#### IV. ASYMPTOTICALLY SAFE BLACK HOLES

In this section, we implement the renormalisation group improvement and analyse the resulting black holes, their horizon structure, and critical Planck-size mini-black holes. The asymptotically safe black hole is obtained by replacing  $G_N$  with the running  $G(r)$  (3.12) in (2.4) and (2.2), leading to the improved, asymptotically safe, lapse function

$$f(r, M) = 1 - G(r, M) \frac{M}{r^{d-3}}. \quad (4.1)$$

At this point we make two observations. The improved Schwarzschild radius  $r_s(M)$  is given by the implicit solution of

$$r_s^{d-3}(M) = M G(r_s(M), M). \quad (4.2)$$

If (4.1) has a solution  $f(r_s(M), M) = 0$ , then it follows that the quantum-corrected horizon is smaller than the classical one  $r_s(M) < r_{\text{cl}}(M)$ . This is a direct consequence of  $G(r, M)/G_N \leq 1$  for all  $r$ . Secondly, if  $G(r, M)/G_N$  decreases too rapidly as a function of  $r$ ,  $f(r_s(M), M) = 0$  will no longer have a real solution  $r_s(M) \geq 0$ , implying the absence of a horizon.

##### A. Horizons

To see the above picture quantitatively, we analyse the horizon condition analytically, also comparing various matching conditions. For a general matching the

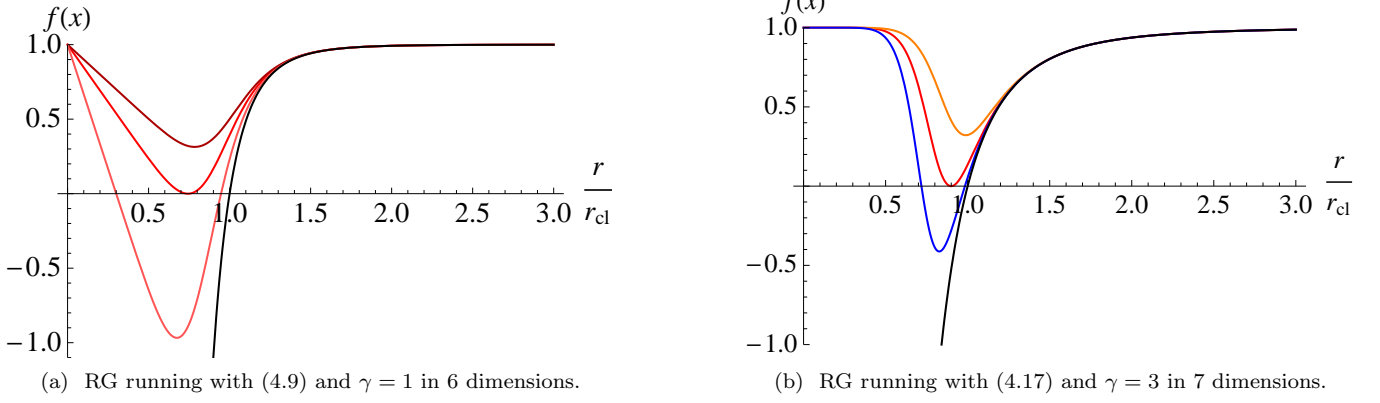


Figure 2: Mass and renormalisation group dependence of the RG improved function  $f(x)$  with  $x = r/r_{\text{cl}}$  in higher dimensions. From top to bottom: absence of horizon  $\Omega > \Omega_c$ , critical black hole  $\Omega = \Omega_c$ , semi-classical black hole  $\Omega < \Omega_c$ , and classical black hole  $\Omega = 0$ .

dimensional analysis (3.13) leads to a running Newton's constant (3.12) of the form

$$\frac{G_0}{G(r)} = 1 + \frac{\tilde{\omega} G_0}{r_{\text{cl}}^{d-2}} \left(\frac{r_{\text{cl}}}{r}\right)^{\gamma(d-2)} \quad (4.3)$$

with  $r_{\text{cl}}$  as in (2.4) and

$$\tilde{\omega} = \omega(\xi/c_\gamma)^{d-2} \quad (4.4)$$

This leads to a lapse function given by

$$f(x) = 1 - \frac{1}{x^{d-3}} \frac{x\gamma^{(d-2)}}{x\gamma^{(d-2)} + \Omega}, \quad (4.5)$$

where we have also introduced the variables

$$x = r/r_{\text{cl}} \quad (4.6)$$

$$r_{\text{cl}} = (M G_0)^{1/(d-3)} \quad (4.7)$$

$$\Omega = \tilde{\omega} (M_D/M)^{\frac{d-2}{d-3}}. \quad (4.8)$$

We define the  $d$ -dimensional Planck mass as  $G_0 = M_D^{2-d}$  corresponding to the convention used by Dimopoulos and Landsberg [6]. The parameter  $\Omega$  captures the RG running of Newton's coupling, and the mass and matching parameter dependence. The classical black hole corresponds to  $\Omega = 0$  which is achieved in the limit of vanishing quantum corrections  $\omega \rightarrow 0$  or in the limit of infinite black hole mass  $M \rightarrow \infty$ . Therefore, the horizon condition  $f(x) = 0$  always includes the classical solution  $x = 1$  at  $r = r_{\text{cl}}$  for  $\Omega = 0$ .

For simplicity, we begin with the case  $\gamma = 1$  corresponding to the IR matching (3.17), where  $f(x)$  takes the form

$$f(x) = 1 - \frac{x}{x^{d-2} + \Omega}. \quad (4.9)$$

For  $\Omega > 0$ , the horizon condition becomes

$$0 = x^{d-3} - 1 + \Omega/x. \quad (4.10)$$

We find three qualitatively different solutions, depending on the value of  $\Omega$  (see Fig. 2(a)). In general, (4.10) has  $d-2$  possibly complex roots  $x(\Omega)$ . For sufficiently small  $\Omega$ , two of these are positive real with  $0 < x_-(\Omega) < x_+(\Omega) \leq 1$  and correspond to a Cauchy horizon  $x_- \equiv r_w/r_{\text{cl}}$  and an outer horizon  $x_+ \equiv r_s/r_{\text{cl}}$ . In even dimensions, the remaining roots are complex conjugate pairs, whereas in odd dimensions, one of the remaining roots is real and negative. Analytical solutions are obtained for  $x_\pm(\Omega)$  as a power series in  $\Omega$  for any  $d > 3$ . With increasing  $\Omega$  (decreasing black hole mass  $M$ ), real solutions to (4.10) cease to exist for  $\Omega > \Omega_c$ . Hence, black hole solutions are restricted to masses  $M$  with

$$\Omega \leq \Omega_c \quad \text{and} \quad M \geq M_c. \quad (4.11)$$

For a black hole of critical mass  $M_c$  we find  $\Omega(M_c) = \Omega_c$ . For such a critical black hole the inner Cauchy horizon and the outer event horizon coincide,  $x_- = x_+ = x_c$  with a radius of  $r_c \equiv x_c r_{\text{cl}}(M_c)$ . Solving  $f(x_c) = 0$  and  $f'(x_c) = 0$  simultaneously leads to the critical parameter

$$\Omega_c = (d-3)(d-2)^{-\frac{d-2}{d-3}} \quad (4.12)$$

$$x_c = (d-2)^{-1/(d-3)}. \quad (4.13)$$

We note that (4.12) is of order one for all  $d \geq 4$ .

Next, we consider the distance function (3.19) whose index  $\gamma$  interpolates between  $\gamma = 1$  for large  $r$  and  $\gamma = \frac{1}{2}(d-1)$  for small  $r$ , similar to the matchings (3.16) and (3.21). We find

$$G(r) = \frac{G_0 r^\alpha}{r^\alpha + \tilde{\omega} G_0 (r_{\text{cl}} + \epsilon r)^{\alpha+2-d}} \quad (4.14)$$

with  $r_{\text{cl}}$  and  $\epsilon$  from (2.4) and (3.20), and

$$\alpha = \frac{1}{2}(d-1)(d-2) \quad (4.15)$$

$$\tilde{\omega} = \omega \xi^{d-2} \left(\frac{d}{2} - \frac{1}{2}\right)^{d-2}. \quad (4.16)$$

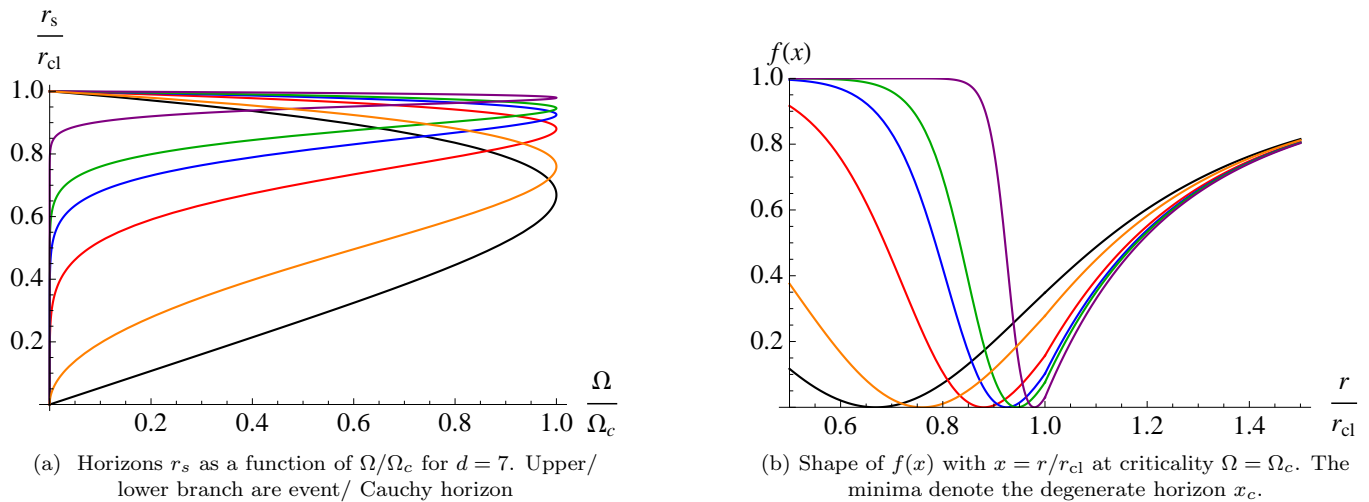


Figure 3: Dependence of Cauchy and event horizon, and of the metric coefficient  $f(x)$  at criticality  $\Omega = \Omega_c$ , on the parameter  $\gamma = 1, \frac{6}{5}, 2, 3, 4$ , and  $10$  [panel (a): from bottom to top, panel (b): from left to right] in  $d = 7$  dimensions. Metric singularities are absent for  $\gamma \geq \gamma_{dS} = \frac{d-1}{d-2}$ . Large values of  $\gamma \rightarrow \infty$  represent the decoupling limit (see text).

Consequently,

$$f(x) = 1 - \frac{x^{\alpha-d+3}}{x^\alpha + \Omega(1+x\epsilon)^{\alpha-d+2}} \quad (4.17)$$

and the horizon condition becomes

$$x^{\alpha-d+3} = x^\alpha + \Omega(1+x\epsilon)^{\alpha-d+2}. \quad (4.18)$$

In Fig. 2(b) we plot (4.17) in  $d = 7$  for three values of  $\Omega$ . The main difference in comparison with Fig. 2(a) is that the limit  $f \rightarrow 1$  is achieved more rapidly.

Finally, we come back to a matching with general index  $\gamma$ , (4.5), with horizon condition

$$0 = 1 - x^{3-d} + \Omega x^{-\gamma(d-2)}. \quad (4.19)$$

Again, three types of solution are found for  $\gamma > \frac{d-3}{d-2}$ , corresponding to two horizons ( $x_+$  and  $x_-$ ) for  $\Omega < \Omega_c$ , none for  $\Omega > \Omega_c$  and a single horizon ( $x_+ = x_- = x_c$ ) for  $\Omega = \Omega_c$ . Solving  $f(x_c) = 0$  and  $f'(x_c) = 0$  simultaneously leads to the critical parameter

$$x_c = \left(1 - \frac{d-3}{\gamma(d-2)}\right)^{\frac{1}{d-3}} \quad (4.20)$$

$$\Omega_c = \frac{d-3}{\gamma(d-2)} \left(1 - \frac{d-3}{\gamma(d-2)}\right)^{\frac{\gamma(d-2)}{d-3}-1}. \quad (4.21)$$

It follows that condition (4.11) will hold independently of the matching used.

Next we discuss the quantitative differences between the various distance functions. This relates to the limit  $r \rightarrow 0$ , where  $f(r)$  approaches  $f \rightarrow 1$ , though with different rates, see Figs. 2. Effectively, the rate is parametrised through  $\gamma$ . We recall that the limit  $\gamma \rightarrow \infty$  switches off

gravity below the horizon  $x_c$ . This entails, in (4.20), that  $x_c \rightarrow 1$ . This is nicely seen in Fig. 3(a) where the horizons are plotted as a function of  $\Omega/\Omega_c$  for various  $\gamma$  with fixed dimensionality  $d = 7$ . In Fig. 3(b), instead, we use (3.14) with  $\gamma = 1$  for  $r > r_{cl}$  and  $\gamma > 1$  for  $r < r_{cl}$ . At  $\Omega = \Omega_c$  we show  $f(r)$  for various  $\gamma$ , and note that the limit  $f \rightarrow 1$  is approached more rapidly for larger values of  $\gamma$ , as expected. We conclude that  $\gamma > 1$  enhances the weakening of gravity in the limit  $r \rightarrow 0$ .

The above findings allow first conclusions. The RG running of  $G(r)$  in the regime where  $r \gg r_{cl}$  has little quantitative influence on the gravitational radius  $r_s$ . Interestingly, the precise RG running in the deep short distance regime  $r \ll r_{cl}$  is also largely irrelevant for the RG improved gravitational radius. Instead, the behaviour of  $G(r)$  and its gradient  $r \partial_r G(r)$  in the regime between  $r \approx r_{cl}$  and  $r \approx r_s$  is mostly responsible for the quantitative shift from  $r_{cl}$  to  $r_s$ . In consequence, the slight differences in the distance functions (3.16), (3.17), (3.18) and (3.19) are attributed to a slight variation in the underlying RG running of  $G(r)$ . The RG results from [20] favour moderate values for  $\gamma$ , as do regularity and minimum sensitivity considerations (see Sec. VD). In all cases studied here, the qualitative behaviour of the horizon structure remains unchanged.

## B. Critical mass

A direct consequence of our results from Sec. IV A is the appearance of a lower bound on the black hole mass below which the RG improved spacetime ceases to have a horizon, see (4.11). The critical mass  $M_c$  is defined implicitly via the simultaneous vanishing of

$f(r_s(M_c), M_c) = 0$  and  $f'(r_s(M_c), M_c) = 0$  (here a prime denotes a derivative with respect to the first argument). Using the solution  $r_s(M)$  of (4.2), we conclude that

$$(d-3)G(r_c, M_c) = r_c G'(r_c, M_c), \quad (4.22)$$

$$r_c = r_s(M_c), \quad (4.23)$$

which serves as a definition for  $M_c$ . The classical limit is achieved for  $M_c \rightarrow 0$ . If  $G(r)$  is a monotonically increasing function of  $r$ , we have  $r\partial_r G(r) \geq 0$ . Then, away from the classical limit, there exists a unique solution  $M_c > 0$  to (4.22). Consequently, the critical mass  $M_c$  is related to the fundamental Planck scale  $M_D$  as

$$M_c = \zeta_c M_D. \quad (4.24)$$

The coefficient  $\zeta_c$  accounts for the renormalisation group improvement of the black hole metric, and hence encodes the RG effects. In the approximation (3.10), (3.13), it reads

$$\zeta_c = \left( \frac{\tilde{\omega}}{\Omega_c} \right)^{\frac{d-3}{d-2}} \quad (4.25)$$

where  $\tilde{\omega} = \omega(\xi/c_\gamma)^{d-2}$ . The link between the RG parameters and the critical mass in units of the fundamental Planck mass  $M_c/M_D$  is displayed in Fig. 4. The location and the number of the horizons depends explicitly on the value of  $\Omega$ , which becomes

$$\Omega = \Omega_c \left( \frac{M_c}{M} \right)^{\frac{d-2}{d-3}} \quad (4.26)$$

in terms of  $M_c$ , see (4.8). Therefore, below, we display our results in terms of  $M_c$ . We return to the discussion of  $M_c$  in Sec. IV G.

### C. Horizons revisited

Next, we return to the quantitative analysis of improved metrics and present our numerical results for the improved Schwarzschild radius.

Figs. 5 6 show how the Schwarzschild radius  $r_s$  depends on the mass of the black hole  $M$  in various dimensions using (3.17). In these plots we considered the scenario where the critical mass  $M_c$  is equal to the Planck mass  $M_D$ . The suppression is less pronounced with increasing dimension (Fig. 5). Also, the deviation from classical behaviour sets in at lower masses in lower dimensions, see Fig. 6(a). Next we consider varying the value of  $M_c$  in units of  $M_D$  while keeping the dimensionality fixed, see Fig. 6(b). The dashed curve corresponds to the classical result. Depending on  $M_c$ , quantum corrected curves start deviating visibly as soon as the black hole mass is only a few  $M_c$  or lower. At fixed  $M/M_D$ , the deviation from classical behaviour sets in earlier for larger  $M_c$ .

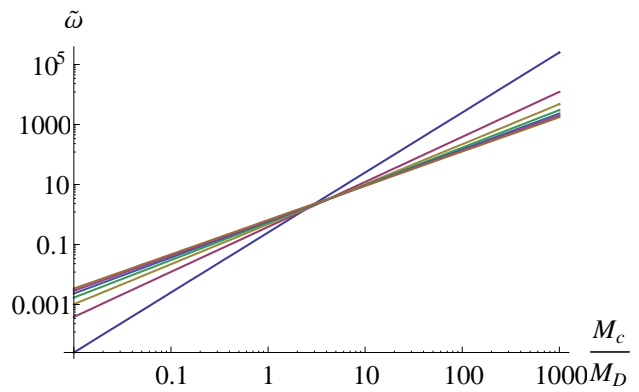


Figure 4: Map between the renormalisation group parameter  $\tilde{\omega}$ , the critical mass  $M_c$ , and the Planck mass  $M_D$ , based on (3.10) and (3.17) for various dimensions. From top to bottom:  $d = 4, 5, \dots, 10$ .

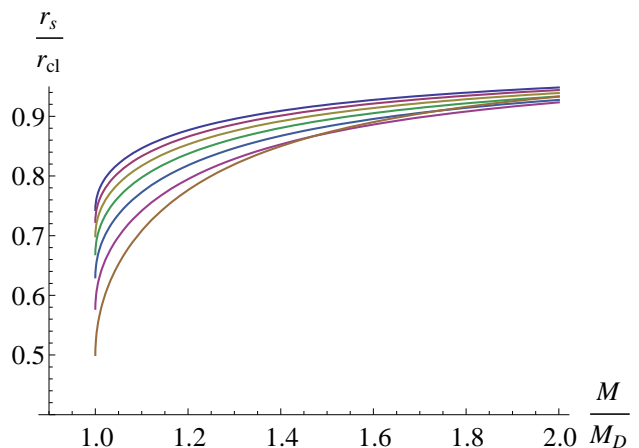


Figure 5: Mass dependence of the improved Schwarzschild radius  $r_s(M)$  compared to its classical value  $r_{cl}(M)$ ;  $M_c = M_D$ . From bottom to top:  $d = 4, 5, \dots, 10$ . The end points denote the critical radii  $r_c$ .

The horizon is slightly sensitive to the distance function (3.11), or equivalently, to the parameter  $\gamma$ . Here,  $\gamma$  parametrises how rapidly  $G(r)$  weakens in the crossover regime at scales  $r \approx r_{cl}$ . This can be seen from Fig 3(a). In the decoupling limit  $\gamma \rightarrow \infty$ , the critical radius  $x_c \rightarrow 1$  reaches the classical value. In this limit, gravity is switched off below  $r_{cl}$ , implying that the Schwarzschild radius remains unchanged. For  $\gamma = 1$ , instead, the outer horizon  $x_+$  decreases rapidly as  $\Omega$  increases towards  $\Omega_c$ .

In conclusion, the quantitative reduction of  $r_s/r_{cl}$  by quantum effects can be associated to the behaviour of the running coupling  $G(r)$  and its decrease  $rG'(r)$  at length scales set by the horizon  $r \approx r_s$ . This decrease, in turn, can be understood via the parameter  $\gamma$  which controls how quickly quantum effects are turned on as  $r/r_{cl}$  becomes small. For all matchings  $k(r) \propto 1/D(r)$  discussed in this paper, and for dimensionality  $d \geq 4$ , the same

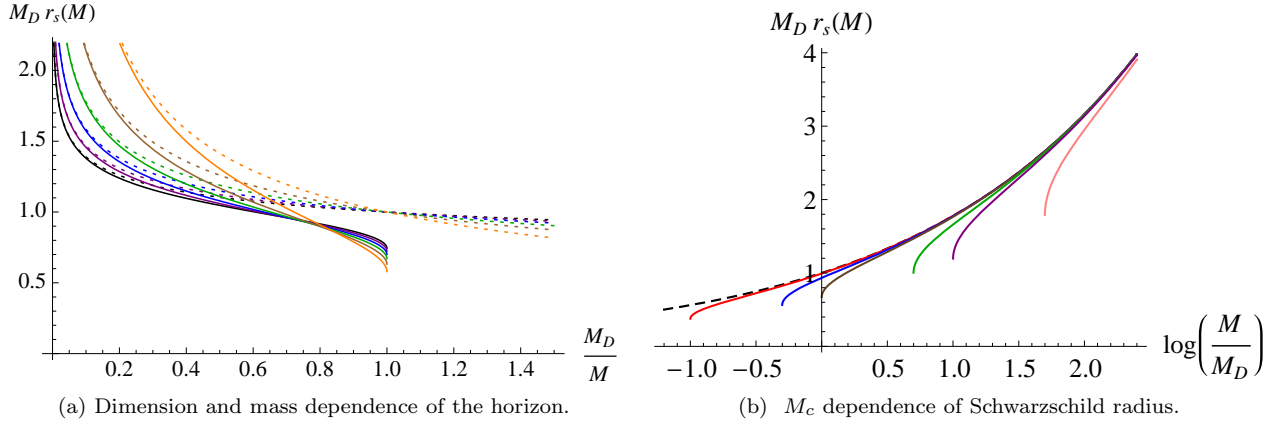


Figure 6: Dependence of the renormalisation group improved Schwarzschild radius  $r_s(M)$  on space-time dimension and critical mass  $M_c$ . End points of curves denote the critical radius  $r_c$  and dashed curves the respective classical result. (a)  $M_c = M_D$  and  $d = 5, 6, \dots, 10$ , from top right to left. (b)  $M_c/M_D = 0.1, 0.5, 1, 5, 10, 50$  from left to right.

qualitative behaviour is observed. In particular the RG improvement indicates that quantum black holes display a lower bound (4.24) of the order of the Planck scale.

#### D. Perturbation theory

In the limit  $M_D/M \ll 1$ , quantum corrections become perturbative and we can perform a large mass expansion. In particular, for asymptotically heavy black holes we find  $x_+ \rightarrow 1$ , as can be seen in Fig. 6(b) where  $r_s$  approaches its classical value for large  $M$  and the dimensionless inner horizon  $x_- \rightarrow 0$  in the large-mass limit. We note that the parameter  $\Omega$  scales as  $\sim M^{-\frac{d-2}{d-3}}$ . Hence a large mass expansion corresponds to an expansion in  $\Omega \ll 1$ . In general, and independently of the RG running and the matching, we find

$$x_{\pm} = \sum_{n=0}^{\infty} a_n^{\pm} \Omega^n \quad (4.27)$$

with dimensionless coefficients  $a_n$ , where  $a_0^+ = 1$  and  $a_0^- = 0$ . The expansion converges rapidly, see Fig. 7. Explicitly, the first few coefficients read

$$x_+ = 1 - \frac{1}{d-3} \Omega - \frac{d-2}{2(d-3)^2} \Omega^2 - \frac{(d-1)(d-2)}{3(d-3)^3} \Omega^3 + O(\Omega^4) \quad (4.28)$$

$$x_- = \Omega + \Omega^{d-2} + (d-2)\Omega^{(2d-5)} + \dots \quad (4.29)$$

using the matching (3.17) and (4.10). The leading order quantum effects modify the Schwarzschild radius  $r_s = x_+ r_{\text{cl}}$  and the Cauchy horizon  $r_w = x_- r_{\text{cl}}$  as

$$r_s = r_{\text{cl}} - \frac{\Omega_c}{d-3} \left( \frac{M_c}{M_D} \right)^{\frac{d-2}{d-3}} \frac{1}{M} + \text{subleading}, \quad (4.30)$$

$$r_w = \Omega_c \left( \frac{M_c}{M_D} \right)^{\frac{d-2}{d-3}} \frac{1}{M} + \text{subleading}. \quad (4.31)$$

Thus, in the limit  $M_D/M \rightarrow 0$  we confirm  $r_s \rightarrow r_{\text{cl}}$  and  $r_w \rightarrow 0$ , as expected.

Interestingly the inner horizon behaves differently if we employ the non-linear matching (3.19). To that end, we again solve the horizon condition, now given by (4.18), and expand in  $\Omega \ll 1$  to find  $x_+$  and  $x_-$  to leading order in  $\Omega$ ,

$$x_+ = 1 - \frac{(1+\epsilon)^{\alpha-d+2}}{d-3} \Omega + \text{subleading} \quad (4.32)$$

$$x_- = \Omega^{\frac{1}{3-d+\alpha}} + \text{subleading} \quad (4.33)$$

where  $\alpha$  and  $\epsilon$  are given by (4.15) and (3.20). We note that if we take  $\alpha = d-2$  we recover (4.28) and (4.29). In the non-linear case the outer horizon  $r_s$  has a large mass expansion similar to (4.30), whereas the inner horizon has a large mass expansion whose leading term is proportional to a positive power of the mass,

$$r_s = r_{\text{cl}} - \frac{\Omega_c(1+\epsilon)^{\alpha-d+2}}{d-3} \left( \frac{M_c}{M_D} \right)^{\frac{d-2}{d-3}} \frac{1}{M} \quad (4.34)$$

$$r_w = \frac{1}{M_D} \left( \frac{M_c \Omega_c}{M_D} \right)^{\rho_0} \left( \frac{M}{M_D} \right)^{\rho_1} \quad (4.35)$$

plus terms subleading in  $M$ . We have introduced  $\rho_0 = \frac{d-2}{(d-3)(\alpha+3-d)}$ ,  $\rho_1 = \frac{5-2d+\alpha}{(d-3)(\alpha+3-d)}$  and  $\rho_1 + \rho_2 = \frac{1}{d-3}$ . For  $d = 4$ ,  $\rho_1 = 0$  for  $d > 4$  we find  $1 > \rho_1 > 0$ . This implies that in the limit  $M \rightarrow \infty$  the Cauchy horizon  $r_w$  will approach a constant for  $d = 4$ . In higher dimensions  $d > 4$ ,  $r_w$  will increase with mass as  $r_w \sim M^{\rho_1}$ , whereas the ratio  $r_w/r_s \sim M^{2-d} \rightarrow 0$  in the large mass limit.

### E. Threshold effects

The RG improved black hole displays an interesting threshold behaviour in the vicinity of  $M \rightarrow M_c$ . This can be understood as follows. Suppose we read (4.1) as a function of  $r$  and  $M$ ,  $f(r, M)$ , and perform a Taylor expansion in both variables. The outcome is then evaluated at the horizon  $r = r_s(M)$  where  $f(r_s(M), M) = 0$ . Independently of the chosen expansion point  $(r_0, M_0)$  with  $r_0 = r_s(M_0)$ , we find

$$0 = \sum_{n=1} \left[ \frac{1}{n!} (M - M_0)^n \frac{\partial^n f}{\partial M^n} + \frac{1}{n!} (r - r_0)^n \frac{\partial^n f}{\partial r^n} \right]$$

at the horizon. Note that the derivatives are evaluated at  $(r, M) = (r_0, M_0)$ . If the RG running of  $G$  is  $M$ -independent, the expansion has only a linear term in  $(M - M_0)$ . At threshold where  $r_0 = r_c$ , we furthermore have  $\partial f / \partial r|_{r_c} = 0$ . In addition,  $\partial f / \partial M|_0$  is always non-zero. Therefore, close to  $M \approx M_c$ ,  $f(r(M), M) = 0$  can only be satisfied if

$$r_s(M) - r_c \sim \sqrt{M - M_c}, \quad (4.36)$$

provided that  $\partial^2 f / \partial r^2|_{r_c} \neq 0$ . More generally, if the first non-vanishing derivative  $\partial^n f / \partial r^n|_{r_c}$  occurs at order  $n$ , the threshold behaviour (4.36) becomes

$$r_s(M) - r_c \sim \sqrt[n]{M - M_c}. \quad (4.37)$$

The generic case encountered in this paper, for all RG runnings employed, is  $n = 2$ . Consequently, at threshold, we have the expansions

$$x_{\pm} = \sum_{n=1}^{\infty} b_n^{\pm} \left( \frac{M}{M_c} - 1 \right)^{n/2} \quad (4.38)$$

with dimensionless coefficients  $b_n^{\pm}$ . This is equivalent to an expansion in powers of  $\sqrt{\Omega_c - \Omega}$ . This expansion converges rapidly as can be seen from Fig. 7, where the first few terms (up to  $n = 6$ ) are enough to match the full solution even for small  $\Omega$ .

Explicitly, using the matching (3.17), the behaviour (4.36) reads to leading order

$$r_s(M) - r_c = \frac{(G_0 M_c)^{1/(d-3)}}{\sqrt{\frac{1}{2}(d-3)M_c}} \sqrt{M - M_c}. \quad (4.39)$$

In the light of the above, the dependence of the horizon radius on the black hole mass can easily be understood, see Fig. 5. For large black hole mass  $M \gg M_c$ ,  $\partial_r f$  is non-vanishing at  $f(r_s) = 0$ , implying that the linear terms in (4.36) have to cancel. This leads to the very soft dependence of  $r_s/r_{cl}$  on  $M_c/M$  for large  $M$ . With decreasing  $M$ ,  $\partial_r f$  is decreasing as well, thereby increasing the admixture from  $(r - r_0)^2$  corrections. The latter

fully take over in the limit  $M \rightarrow M_c$ , leading to non-analytical behaviour (4.36) which is nicely seen in Fig. 5. We stress that this structure is independent of the dimension as long as  $d > 3$ .

### F. Temperature and specific heat

The threshold behaviour of Sec. IV E has important implications for the thermodynamics of black holes. Based on the RG improvement used here, the Bekenstein-Hawking temperature is given by [60, 61]

$$T = \frac{f'(r_s(M), M)}{4\pi}, \quad (4.40)$$

where the prime denotes a derivative with respect to the first argument. We conclude that the temperature is bounded,  $T(M) \leq T_{cl}(M)$ . Equality is achieved for asymptotically large black hole mass, where the temperature scales inversely with mass,  $T \sim 1/M$ , and the specific heat

$$C = \frac{\partial M}{\partial T} \quad (4.41)$$

is negative. In this regime, it is expected that the black hole evaporates through the emission of Hawking radiation, thereby lowering its mass through the influx of negative energy. At threshold with  $M \rightarrow M_c$ , however, the black hole temperature vanishes because  $f'(r_c) \rightarrow 0$ . In the vicinity of  $M \approx M_c$ , the temperature of the black hole scales non-analytically,

$$\frac{\partial T}{\partial M} \sim \frac{\partial r_s(M)}{\partial M} \sim \frac{1}{\sqrt{M - M_c}} > 0 \quad (4.42)$$

as a consequence of (4.36). Therefore, the specific heat has become positive, and the temperature displays a maximum  $T(M) \leq T_{\max}$  for all  $M$ . Furthermore, since  $\partial T / \partial M$  vanishes at  $T_{\max}$ , the specific heat changes its sign through a pole. We conjecture that black holes with mass  $M_c$  constitute cold remnants, provided they can be reached through an evaporation process. This would require, however, that  $T_{\max}$  remains below the fundamental Planck scale.

### G. Renormalisation and the Planck scale

We summarise our results. The main physics of this paper originates from a new mass scale  $M_c$ , which is absent in the classical theory. Its existence is due to quantum gravity corrections, implemented on the level of the metric.

For black hole mass  $M$  large compared to  $M_c$ , renormalisation group corrections to the metric are small. The

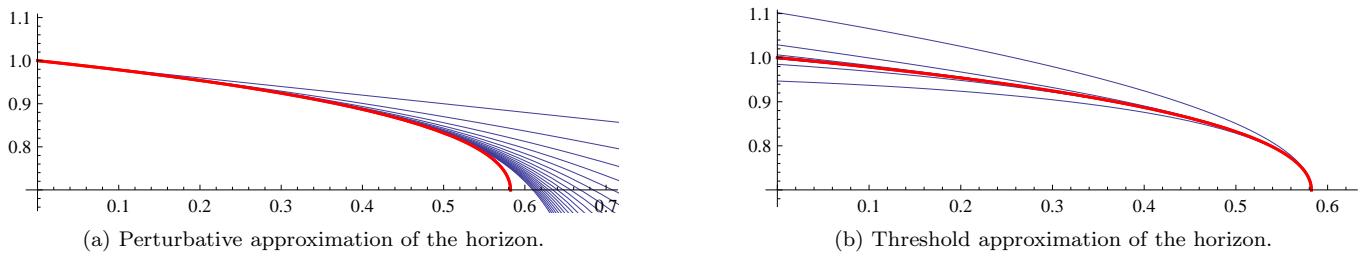


Figure 7: Location of the event horizon  $x_+(\Omega) \equiv r_s/r_{\text{cl}}$  as a function of the parameter  $\Omega$  in  $d = 8$  (thick line) within various approximations (thin lines). (a) Perturbative expansion about  $\Omega = 0$  using (4.27) at order  $n = 1, 2, \dots, 20$ , approaching the exact solution adiabatically (from top to bottom). (b) Threshold expansion about the critical point  $\Omega = \Omega_c$  using (4.38) at order  $n = 1, 2, \dots, 9$ , alternating towards the full solution.

gravitational force remains strong enough to allow for black holes. Improved black hole metrics display horizons of the order of the classical horizon, the specific heat stays negative and the temperature scale inversely proportional to mass, modulo small quantum corrections. This is the semi-classical regime of the theory.

Once the mass  $M$  approaches  $M_c$ , we observe the transition from strong to weak gravity. In its vicinity, renormalisation effects become of order one, the reduction of the event horizon becomes more pronounced, the specific heat has become positive and the thermodynamical properties are no longer semi-classical. This is the Planckian (or quantum) regime of the theory.

When  $M$  drops below  $M_c$ , renormalisation group corrections to the metric have become strong. The gravitational force has weakened significantly, to the point that improved black hole space-times no longer display a horizon. This is the deep UV scaling regime of the theory. The improved metric differs qualitatively from the classical one. Hence, the applicability of our renormalisation group improvement becomes doubtful, and conclusions from this regime have to be taken with care.

If the renormalisation effects of the black hole space-time are parametrically strong,  $\tilde{\omega} \gg 1$ , the scale  $M_c$  grows large, and parametrically larger than the Planck scale  $M_D$ . In turn, for weak renormalisation  $\tilde{\omega} \ll 1$ , the scale  $M_c$  remains small as well. We note that  $M_c$  vanishes in the classical limit where quantum corrections are switched off. The reason for this is that the Schwarzschild solution of classical general relativity does not predict its own limit of validity under quantum corrections. Interestingly, the underlying fixed point is not primarily responsible for the existence of the lower bound  $M_c$ . Other ultraviolet completions of gravity such as string theory, loop quantum gravity or non-commutative geometry can lead a similar weakening of the gravitational force at length scales of the order of the Planck length.

To conclude, the improved metric changes qualitatively at  $M \approx M_c$ . Therefore it is tempting to interpret  $M_c$  as a ‘renormalised’ Planck scale. Its numerical value depends

on the precise renormalisation group running. As long as the latter is driven by the gravitational self-coupling only, it is natural to have  $M_c$  of the order of  $M_D$ . This may be different once strong renormalisation effects are induced by external mechanisms, eg. through the coupling to a large number of matter fields.

## V. SPACE-TIME STRUCTURE AND PENROSE DIAGRAM

In this section, we study the implications of quantum gravitational effects on the space-time structure of black holes, including a discussion of critical black holes, an analogy with Reissner-Nordström black holes, an interpretation in terms of an effective energy momentum tensor, the (absence of) curvature singularities at the origin, and the causality structure and Penrose diagram of quantum black holes.

### A. Critical black holes

The space-time structure of a critical black hole with mass  $M = M_c$  has a single horizon at  $r_c = r_{\text{cl}} x_c$  and  $x_- = x_+ = x_c$  where the function  $f(x)$  has a double zero  $f(x_c) = 0$ . For the matching (3.17)  $x_c$  is given explicitly by (4.13). The near-horizon geometry of a critical black hole is obtained by expanding  $f(x)$  around  $x = x_c$ . We find

$$f(x) = \frac{1}{2} \bar{x}^2 f''(x_c, \Omega_c) \quad (5.1)$$

where  $\bar{x} \equiv x - x_c$  and the double prime represents a second derivative with respect to  $x$ . Therefore, we can write the line element in terms of the coordinate  $\bar{r} = r - r_c$  as

$$ds^2 = -\frac{\bar{r}^2}{r_{\text{AdS}}^2} dt^2 + \frac{r_{\text{AdS}}^2}{\bar{r}^2} d\bar{r}^2 + r_c^2 d\Omega_{d-2}^2 \quad (5.2)$$

The metric (5.2) is the product of a two-dimensional anti-de Sitter space with a  $(d-2)$ -sphere,  $\text{AdS}_2 \times S^{d-2}$ , and depends on their respective radii

$$r_{\text{AdS}} = (G_0 M_{\text{AdS}})^{1/(d-3)} \quad (5.3)$$

$$r_c = x_c (G_0 M_c)^{1/(d-3)} \quad (5.4)$$

The curvature of the anti-de Sitter part is determined by the mass parameter  $M_{\text{AdS}}$ ,

$$M_{\text{AdS}} = M_c \left( \frac{1}{2} f''(x_c, \Omega_c) \right)^{-\frac{1}{2}(d-3)}. \quad (5.5)$$

Using (3.17) for  $d = 4$  we have  $M_{\text{AdS}} = \frac{1}{\sqrt{2}} M_c$ . For higher dimensions  $d = 6, 8, 10$  we find  $M_{\text{AdS}}/M_c \approx 0.14, 0.017, 0.0016$ , respectively. For all dimensions, we have  $M_{\text{AdS}} < M_c$ . We note that the metric (5.2) is of the form of a Robinson-Bertotti metric for a constant electric field.

## B. Reissner-Nordström-type metrics

It is interesting to compare the RG improved black hole with the well-known Reissner-Nordström solution of a charged black hole in higher dimensions [29]. The latter is defined via the lapse function

$$f_{\text{RN}}(r) = 1 - \frac{G_0 M}{r^{d-3}} + \frac{G_0 e^2}{r^{2(d-3)}} \quad (5.6)$$

where  $e^2$  denotes the charge of the black hole (squared). The charge has the mass dimension  $[e^2] = 4 - d$ . The physics of the Reissner-Nordström black hole is best understood in terms of the dimensionless parameter

$$\Omega_{\text{RN}} = \frac{e^2}{G_0 M^2} \quad (5.7)$$

which measures the relative strength of the competing terms on the rhs of (5.6). In terms of (5.7) and using  $x = r/r_{\text{cl}}$ , the lapse function becomes

$$f_{\text{RN}}(x) = 1 - \frac{1}{x^{d-3}} + \frac{\Omega_{\text{RN}}}{x^{2d-6}}. \quad (5.8)$$

For  $\Omega_{\text{RN}} > \frac{1}{4}$  the spacetime has no horizons and exhibits a naked singularity. For  $\Omega_{\text{RN}} < \frac{1}{4}$  the spacetime displays two horizons, whereas for  $\Omega_{\text{RN}} = \frac{1}{4}$  the black hole displays a single horizon. Therefore  $\Omega_{\text{RN}} = \frac{1}{4}$  is referred to as an extremal black hole with critical mass  $M_{\text{RN},c} = 2\sqrt{e^2/G_0}$ . The radius of the extremal black hole is given by  $r_{\text{RN},c} = 2^{-1/(d-3)} r_{\text{cl}}$ .

Reissner-Nordström spacetimes share some of the qualitative features of RG improved higher dimensional black holes discussed in this paper. If we consider a quantum black hole using the matching (3.17) and expand the lapse function to leading order in  $\Omega$ , we find

$$f_{\text{LO}}(x) = 1 - \frac{1}{x^{d-3}} + \frac{\Omega}{x^{2d-5}} + \text{subleading}. \quad (5.9)$$

In either case (5.8) and (5.9), the relevant physics originates from competing effects: a leading order Schwarzschild term  $-1/r^{d-3}$ , which is counterbalanced by either the charge, parametrised by  $\Omega_{\text{RN}} \sim e^2$ , or by quantum corrections due to a running gravitational coupling, parametrised by  $\Omega \sim \tilde{\omega}$ . The correction terms become quantitatively dominant with decreasing  $r \rightarrow 0$ . We note that (5.8) and (5.9) are formally equal for  $\Omega_{\text{RN}} = \Omega x$ . In either case, in the large mass limit  $M \rightarrow \infty$  we find an outer horizon  $f(x_+) = 0$  for  $x \approx 1$ . It follows that the near horizon geometry of a quantum black hole is approximately that of a Reissner-Nordström black hole of charge  $e^2 = \tilde{\omega} r_{\text{cl}}^{d-4}$ , and in the large mass limit.

Next we consider the near horizon geometry of an extremal Reissner-Nordström black hole, which is of the  $\text{AdS}_2 \times S^{d-2}$  type. The line element is given by (5.2) where

$$r_c = \left( \frac{1}{2} G_0 M_{\text{RN},c} \right)^{1/(d-3)} \quad (5.10)$$

$$M_{\text{AdS}} = M_{\text{RN},c} \left( \frac{1}{2} f''_{\text{RN}}(x_c, \Omega_c) \right)^{-(d-3)/2}. \quad (5.11)$$

For  $d = 4$  we find  $M_{\text{AdS}} = \frac{1}{2} M_{\text{RN},c}$ . For higher dimensions  $d = 6, 8$  and  $10$ , we obtain  $M_{\text{AdS}}/M_{\text{RN},c} \approx 0.02, 0.0002$  and  $6 \times 10^{-7}$ , respectively. The decreasing of  $M_{\text{AdS}}/M_{\text{RN},c}$  with dimension is similar to the decreasing of  $M_{\text{AdS}}/M_c$  for the critical black hole (5.5).

## C. Effective energy-momentum tensor

In this paper we have obtained our results by replacing the classical value of Newton's constant  $G_0$  with a running constant  $G(r)$ . It is interesting to ask whether this modification could have arisen from an explicit source term, the energy-momentum tensor, for Einstein's equations. The answer is affirmative, and obtained by inserting the RG improved metric into the left hand side of the Einstein equations  $G^{\mu\nu} = 8\pi G_0 T^{\mu\nu}$ . The non-vanishing components are the diagonal ones  $T^\mu_\nu = \text{diag}(-\rho, p_r, p_\perp, \dots, p_\perp)$ , given by

$$\rho = -p_r = \frac{G'(r) M_{\text{phys}}}{S_{d-2} G_0 r^{d-2}} \quad (5.12)$$

$$p_\perp = -\frac{G''(r) M_{\text{phys}}}{(d-2) S_{d-2} G_0 r^{d-3}} \quad (5.13)$$

where  $S_{d-2} = 2\pi^{(d-1)/2}/\Gamma((d-1)/2)$ . Integrating the energy density  $\rho$  over a volume of radius  $r$  one finds the effective energy within that radius,

$$E(r) = S_{d-2} \int_0^r dr' \rho(r') r'^{d-2} = \frac{G(r) M_{\text{phys}}}{G_0}, \quad (5.14)$$

where we assume  $G(r)$  obeys the limits  $G(r) \rightarrow 0$  for  $r \rightarrow 0$  and  $G \rightarrow G_0$  for  $r \rightarrow \infty$ . As such we note that  $E(\infty) = M_{\text{phys}}$  the physical mass. We also make the observation that replacing  $G(r) M_{\text{phys}} \rightarrow G_0 E(r)$  leaves the metric invariant.

#### D. Absence of curvature singularities

In this section, we discuss the  $r \rightarrow 0$  limit of asymptotically safe black holes and the absence of curvature singularities. Classical Schwarzschild solutions display a coordinate singularity at  $r = r_{\text{cl}}$  where  $f(r)^{-1} \rightarrow \infty$ . Curvature invariants remain well-defined and finite at the horizon, which shows that the singularity is only an apparent one.

A curvature singularity in the classical metric is found at  $r \rightarrow 0$ , where  $f(r) \rightarrow -\infty$  and the Ricci scalar diverges as  $R \sim r^{1-d}$ . This curvature singularity implies the break-down of classical physics at the centre of a black hole. It is expected that quantum fluctuations should lead to a less singular or finite behaviour as  $r \rightarrow 0$ .

Within the renormalisation group set-up studied here, the main new input is the anti-screening of the gravitational coupling. Consequently,  $G(r)/G_N$  becomes very small, thereby modifying the  $r \rightarrow 0$  limit. For small  $r/r_{\text{cl}} \ll 1$ , we have

$$f(r) = 1 - (\mu r)^\sigma + \text{subleading} \quad (5.15)$$

where the mass scale  $\mu$  and the parameter  $\sigma$  are fixed by the renormalisation group and the matching condition discussed in Sec. III. We note that a value of  $\sigma = 2$  would correspond to a de Sitter core with cosmological constant

$$\Lambda_{\text{dS}} = \frac{1}{2}(d-1)(d-2)\mu^2. \quad (5.16)$$

More generally, the value of  $\sigma$  depends on the detailed short distance behaviour. We find  $\sigma_{\text{ir}} = 1$  using (3.17) for all values of  $d \geq 4$ , and  $\sigma_{\text{uv}} = \frac{1}{2}(d^2 - 5d + 8)$  using (3.18). For  $d \geq 4$  the latter takes values  $\sigma_{\text{uv}} \geq 2$ . In contrast to this, the classical solution displays  $\sigma_{\text{cl}} = 3-d$ . Using the matching (3.13) with parameter  $\gamma$  we have  $\sigma = \gamma(d-2) - d + 3$ . Consequently, a de Sitter core is achieved for

$$\gamma_{\text{dS}} = (d-1)/(d-2) \quad (5.17)$$

in the limit  $r \rightarrow 0$ .

Next, we calculate the Ricci scalar, the Riemann tensor squared and the Weyl tensor squared in the limit  $r \rightarrow 0$ , using (5.15). The results are

$$\begin{aligned} R &= F_R \cdot (\mu r)^{\sigma-2} \mu^2 \\ R^{\mu\nu\kappa\lambda} R_{\mu\nu\kappa\lambda} &= F_{\text{Riem}} \cdot (\mu r)^{2\sigma-4} \mu^4 \\ C^{\mu\nu\kappa\lambda} C_{\mu\nu\kappa\lambda} &= F_C \cdot (\mu r)^{2\sigma-4} \mu^4 \end{aligned} \quad (5.18)$$

modulo subleading corrections. The coefficients are

$$\begin{aligned} F_R &= (\sigma + d - 2)(\sigma + d - 3) \\ F_{\text{Riem}} &= \sigma^4 - 2\sigma^3 + (2d - 3)\sigma^2 + 2(d - 2)(d - 3) \\ F_C &= \frac{d - 3}{d - 1}(\sigma - 1)^2(\sigma - 2)^2 \end{aligned} \quad (5.19)$$

Clearly, the curvature singularity is absent as soon as  $\sigma \geq 2$ , which in general is achieved for the matchings employed here including (3.18). For the matching (3.17), however, we have  $\sigma = 1$  and conclude that in this case the remaining curvature singularity reads  $R \sim \frac{1}{r}$ . This is still a significant reduction in comparison with the behaviour  $\sim r^{1-d}$  within the classical Schwarzschild solution, and indicates that the weakening of gravitational interactions leads to a better short distance behaviour.

The Riemann-squared coefficient is non-zero for all values of  $\sigma$  when  $d \geq 4$ . The Weyl-squared term has the same  $r$ -dependence as the Riemann-squared term, but its coefficient vanishes for both  $\sigma = 1$  and  $\sigma = 2$ . Hence, there is no choice for  $\sigma$  which makes all three coefficients vanishing.

We are lead to the following conclusions. Regularity of an asymptotically safe black hole requires  $\sigma \geq 2$ . The RG study indicates that the behaviour for the physical theory lies in between the limits set by  $\sigma_{\text{ir}} \leq \sigma_{\text{phys}} \leq \sigma_{\text{uv}}$ . It is tempting to speculate that the physical value would read  $\sigma = 2$  corresponding to a de Sitter core with positive cosmological constant set by (5.16). A distance function with effective index  $\gamma \geq \gamma_{\text{dS}}$  together with a momentum-scale RG for Newton's coupling provides for a singularity-free metric for all  $r$ . This is a very mild constraint on the RG running, as  $\gamma_{\text{dS}} \in [1, \frac{3}{2}]$  is very close to  $\gamma_{\text{ir}} = 1$  for all  $d \geq 4$ .

As a last observation, we treat  $\gamma$  as a free parameter and employ a principle of minimum sensitivity (PMS) condition to identify its best match value  $\gamma_{\text{PMS}}$  [62]. Since the horizon radius  $r_s = r_s(\gamma)$  at fixed black hole mass depends monotonically on  $\gamma$ , a PMS condition singles out the boundaries of the parameter space given by the decoupling limit  $1/\gamma \rightarrow 0$ , and the de Sitter limit  $\gamma = \gamma_{\text{dS}}$ . The decoupling limit corresponds to the switching-off of gravity. Hence, we conclude that a minimum sensitivity condition singles out  $\gamma_{\text{PMS}} = \gamma_{\text{dS}}$ .

#### E. Kruskal-Szekeres coordinates

In this section we introduce Kruskal-Szekeres coordinates which remove the coordinate singularities at the horizons. This is the first step towards a discussion of the causal structure of asymptotically safe black holes and their Penrose diagrams.

Here we consider the case where  $M > M_c$  such that the spacetime has two horizons; the outer horizon  $r_s \equiv r_{\text{cl}+}$

and the Cauchy horizon  $r_w \equiv r_{\text{cl}} x_-$ . For simplicity we will consider the linear matching (3.17) where the lapse function is given by (4.9) such that  $\alpha = d - 2$ . The horizons are found by the real positive roots of (4.10). In general there will be exactly  $\alpha = d - 2$ , possibly complex, roots. In the regime of interest where  $0 < \Omega < \Omega_c$ , we have always two real positive roots  $x_{\pm}$ . In even or odd dimensions, we additionally find  $(d - 4)/2$  pairs of complex conjugate roots, or a real negative root and  $(d - 5)/2$  pairs of complex conjugate roots, respectively. Therefore, we decompose

$$\begin{aligned} \Delta &\equiv x^\alpha + \Omega - x \\ &= (x - x_+)(x - x_-) \prod_{i=1}^{\alpha-2} (x - z_i). \end{aligned} \quad (5.20)$$

into the two real roots  $x_{\pm} > 0$  and the remaining  $d - 4$  roots  $z_i$ . In terms of these, we have

$$\Omega = (-1)^\alpha x_+ x_- \prod_{i=1}^{\alpha-2} z_i. \quad (5.21)$$

We express the line element in terms of the roots and the dimensionless radial coordinate  $x$

$$ds^2 = -\frac{\Delta}{x^\alpha + \Omega} dt^2 + \frac{x^\alpha + \Omega}{\Delta} dr^2 + r^2 d\Omega_{d-2}^2. \quad (5.22)$$

Next we express the line element in terms of Kruskal-Szekeres type coordinates to remove the coordinate singularities. We will follow the method as outlined in [63] for a Reissner-Nordström black hole with two horizons. First we define the dimensionless tortoise coordinate

$$dx^* = \frac{x^\alpha + \Omega}{\Delta} dx \quad (5.23)$$

It is then clear that radial null geodesics correspond to  $t/r_{\text{cl}} = \pm x^*$ . Performing the integral we find

$$\begin{aligned} x^* &= x + \frac{1}{2\kappa_+} \ln(|x - x_+|) + \frac{1}{2\kappa_-} \ln(|x - x_-|) \\ &+ \sum_{i=1}^{\alpha-2} \frac{1}{2\kappa_i} \ln((x - z_i)) + \text{constant} \end{aligned} \quad (5.24)$$

$$\kappa_i = \frac{(z_i - x_+)(z_i - x_-) \prod_{j \neq i}^{\alpha-2} (z_i - z_j)}{2z_i} \quad (5.25)$$

$$\kappa_+ = \frac{(x_+ - x_-) \prod_{j=1}^{\alpha-2} (x_+ - z_j)}{2x_+} \quad (5.26)$$

$$\kappa_- = \frac{(x_- - x_+) \prod_{j=1}^{\alpha-2} (x_- - z_j)}{2x_-} \quad (5.27)$$

We now introduce advanced and retarded time coordinates given by

$$v = x^* + w \quad (5.28)$$

$$u = x^* - w \quad (5.29)$$

where  $w$  is the dimensionless time  $w \equiv t/r_{\text{cl}}$ . We then define the coordinates

$$V^\pm = e^{\kappa_\pm w} \quad (5.30)$$

$$U^\pm = -e^{-\kappa_\pm w} \quad (5.31)$$

These are the KS-type coordinates for quantum black holes. The product

$$U^\pm V^\pm = -e^{2\kappa_\pm x^*} \quad (5.32)$$

is a constant for any given radius  $x$ . In terms of the coordinates  $U^+$  and  $V^+$  the line element becomes

$$\begin{aligned} ds^2 &= -\left(\frac{r_{\text{cl}}}{\kappa_+}\right)^2 e^{-2\kappa_+ x^*} \frac{\Delta}{x^\alpha + \Omega} dU^+ dV^+ \\ &+ r^2 d\Omega_{d-2}^2 \end{aligned} \quad (5.33)$$

Inserting  $x^*$  given by (5.24) we find

$$ds^2 = -r_{\text{cl}}^2 F_+(x) dU^+ dV^+ + r^2 d\Omega_{d-2}^2 \quad (5.34)$$

$$F_+ = \frac{e^{-\kappa_+ x} \kappa_+^{-2} (x - x_-)}{x^\alpha + \Omega} \prod_{i=1}^{\alpha-2} \frac{x - z_i}{(x - z_i)^{\frac{\kappa_+}{\kappa_i}}}. \quad (5.35)$$

The singularity in the  $x_+$  coordinate has been removed and the metric covers regions of space time for  $x > x_-$ . There remains a singularity at  $x = x_-$ , and, therefore, the metric does not cover the region  $x \leq x_-$ . Instead we use the coordinates  $U^-$  and  $V^-$  in terms of which the line element is given by

$$ds^2 = -r_{\text{cl}}^2 F_-(x) dU^- dV^- + r^2 d\Omega_{d-2}^2 \quad (5.36)$$

$$F_- = \frac{e^{-\kappa_+ x} \kappa_-^{-2} (x - x_+)}{x^\alpha + \Omega} \prod_{i=1}^{\alpha-2} \frac{x - z_i}{(x - z_i)^{\frac{\kappa_-}{\kappa_i}}}. \quad (5.37)$$

Hence the singularity at  $x = x_-$  is removed in these coordinates and the metric is well defined in the region  $x < x_+$ . The singularity at  $x = x_+$  remains in this parametrisation and does not cover the region  $x > x_+$ . The coordinates (5.30) are defined such that for ingoing null rays  $V^\pm = \text{constant}$  and for outgoing null rays  $U^\pm = \text{constant}$ .

## F. Causality and Penrose diagram

The global structure of the black hole can be represented by a Penrose diagram. To produce the diagram we make an analytical continuation of the KS-type coordinates and then map them to a finite interval

$$V^\pm \rightarrow \tanh(V^\pm) \quad (5.38)$$

$$U^\pm \rightarrow \tanh(U^\pm). \quad (5.39)$$

The resulting Penrose diagram is shown in Fig. 8. The causal structure can be understood by noting that null

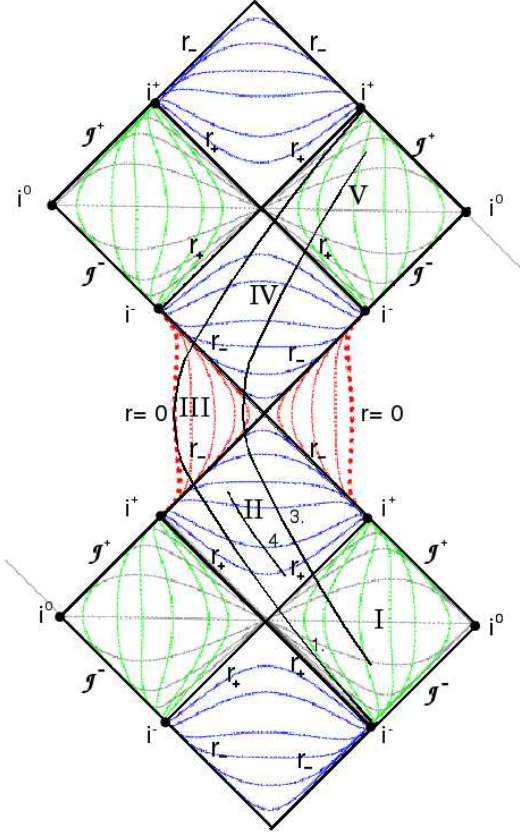


Figure 8: The Penrose diagram of a quantum black hole with  $M > M_c$ . The black curves in regions I and V are curves of constant  $t$ . The green (blue) [red] curves are curves of constant  $r$  in region I and V (II and IV) [III], respectively. In- and outgoing radial null geodesics are at  $45^\circ$ . Curves 1., 3. and 4. correspond to schematic plots of various solutions to the equations of motion. The points  $i^0$ ,  $i^+$  and  $i^-$  denote spatial infinity, future infinity and past infinity, respectively.  $\mathcal{J}^-$  and  $\mathcal{J}^+$  denote past and future null infinity (see text).

geodesics are always at  $45^\circ$  such that ingoing photons point “north-west” and outgoing photons point “north-east”. Regions I, II and III correspond to  $x > x_+$ ,  $x_- < x < x_+$  and  $x < x_-$ , respectively, where  $x_+$  denotes the outer horizon and  $x_-$  the inner Cauchy horizon in units of  $r_{cl}$ . The other regions are the analytical continuations; in particular regions IV and V correspond

to  $x_- < x < x_+$  and  $x > x_+$ . Surfaces of constant  $r$  in region II ( $x_- < x < x_+$ ) are trapped surfaces such that all null geodesics move towards the inner horizon. On the other hand region IV defines a white hole where all null geodesics point towards  $r_+$ .

To get an idea of the causal structure experienced by an in-falling observer we follow the standard procedure of considering a radially moving test particle as was done in the  $d = 4$  case [22]. We define the dimensionless proper time of the radial particle  $d\tau^2 = ds^2/r_{cl}^2$ . A constant of motion  $\zeta$  is defined by the Killing vector equation corresponding to the time independent nature of the metric,

$$\zeta = f(x) \frac{dw}{d\tau}. \quad (5.40)$$

From the form of the metric (2.1) the equations of motion for the test particle can then be given in terms of  $\zeta$ :

$$\dot{x}^2 = \zeta^2 - f(x) \quad (5.41)$$

(dots denote derivatives with respect to proper time  $\tau$ .) We define a Newtonian-like potential,  $\Phi(x) = \frac{1}{2}(f(x)-1)$ , to write an equation for the proper acceleration of the test particle

$$\ddot{x} = -\frac{\partial\Phi(x)}{\partial x}. \quad (5.42)$$

This equation can be checked by differentiating (5.41) with respect to  $\tau$ . For the linear matching (3.17) the proper acceleration is given by,

$$\ddot{x} = -\frac{1}{2} \frac{(d-3)x^{d-2} - \Omega}{(x^{d-2} + \Omega)^2}. \quad (5.43)$$

From (5.41) write down an “energy” equation:

$$E \equiv \frac{\zeta^2 - 1}{2} = \frac{1}{2}\dot{x}^2 + \Phi(x) \quad (5.44)$$

For different values of  $E$  we analyse various solutions to the equations of motion for radially moving test particles. The potential takes its maximum value  $\Phi_{max} = 0$  at  $r = 0, \infty$  and, for  $M > M_c$ , its minimum value will be  $\Phi_{min} < -\frac{1}{2}$ . The different solutions discussed below are shown as curves in Fig. 8.

1. For  $E = 0$  the particle has zero velocity at  $r = 0$  and  $r = \infty$ . For the linear matching the particle will start in region I with a non-zero velocity and cross the horizons into regions II and III in a finite proper time. The particle will then reach the centre of the black hole where it feels a repulsive force with a strength of  $1/(2r_s\Omega)$ . This force will bounce the particle back into regions IV and V where it will escape to infinity.

2. For  $E > 0$  the motion of the particle will be unbounded since it has a non-zero velocity at all points in spacetime. Starting from region I the particle will again move to the centre of the black hole crossing both horizons in a finite time  $\tau$ . But at  $r = 0$  the particles energy will be enough to overcome the repulsive force and will pass through the centre of the black hole into regions IV and V where it will escape to infinity.
3. For  $-0.5 < E < 0$  the particle starts with zero velocity in region I and continues to move into regions II and then into III where it has an inflection at  $r > 0$ . Here the particle is bounced into regions IV and V. In region V it has a second inflection point at a radius equal to it's initial position in region I. The particle's motion is therefore bounded moving in and out of the black hole into different regions of spacetime.
4. For  $\Phi_{min} < E < -0.5$  the particle's motion is bound to region II in which it has two inflection points which it moves between eternally.

A discussion of causal structures, taking into account the time-dependent evaporation effects of asymptotically safe black holes, will be summarised elsewhere [17].

## VI. BLACK HOLE PRODUCTION

In this section, we apply our results to the production of mini-black holes in higher-dimensional particle physics models of TeV scale quantum gravity.

### A. Large extra dimensions

The scenario of large extra dimensions assumes that gravity propagates in  $d = 4 + n$  dimensions, whereas matter fields are confined to a four-dimensional brane [3]. The  $n$  extra dimensions are compactified with compactification radius  $L$ . For simplicity, we assume that all radii are of the same order of magnitude, which can be relaxed if required. The presence of extra dimensions allows for a fundamental  $d$ -dimensional Planck scale  $M_D$  of the order of the electroweak scale  $\sim 1\text{TeV}$ . The relationship between the effective 4-dimensional Planck scale  $M_{\text{Pl}}$  and the  $d$ -dimensional Planck scale is given by

$$M_{\text{Pl}}^2 \approx M_D^2 (M_D L)^n. \quad (6.1)$$

Furthermore, we require the scale-separation  $M_D L \gg 1$  to achieve a low fundamental quantum gravity scale. This implies that the length scale  $L$  at which the extra dimensions become visible is much larger than the fundamental length scale  $1/M_D$  at which the quantum gravity

effects become important. Consequently, at energy scales  $E \approx M_D$ , the full  $d$ -dimensional space-time is accessible to gravity, and our previous findings are applicable.

### B. Production cross section

Here, we apply our results [17] to the production cross section for mini-black holes at particle colliders. In these models, the elastic black hole production cross section for parton-parton scattering at trans-Planckian center-of-mass energies  $\sqrt{s} \gg M_D$  is semi-classical, provided curvature effects are small [6–9, 64]. Then, on the parton level, the geometric cross section reads

$$\hat{\sigma}_{\text{cl}}(s) \approx \pi r_{\text{cl}}^2(M_{\text{phys}} = \sqrt{s}) \theta(\sqrt{s} - M_{\text{min}}), \quad (6.2)$$

with the physical mass replaced by the center-of-mass energy  $\sqrt{s}$ . There are formation factor corrections to (6.2) which have been identified in the literature, taking into account inefficiencies in the production process (see [10] for reviews). Those have not been written out explicitly as they are irrelevant to our reasoning. For phenomenological applications, it is often assumed that the minimal mass  $M_{\text{min}}$  is of the order of a few  $M_D$ , limiting the regime where the semi-classical theory is applicable.

Our study adds two elements to the picture. The first one relates to the threshold mass, indicating that  $M_{\text{min}}$  may in fact be lower, possibly as low as the renormalised Planck mass

$$M_{\text{min}} = M_c. \quad (6.3)$$

This is a direct consequence of the RG running of the gravitational coupling, with  $M_c$  relating to the critical physical mass (defined as in (2.3)), thereby marking a strict lower limit for the present scenario. Consequently, the RG improved set-up has a larger domain of validity due to the weakening of gravity at shorter distances, equally reflected in the boundedness of the associated Bekenstein-Hawking temperature, see Sec. IV F.

The second modification takes the quantum gravity-induced reduction of the event horizon into account, replacing  $r_{\text{cl}}$  by  $r_s$  in (6.2). This can be written in terms of a form factor, replacing (6.2) by  $\hat{\sigma} = \hat{\sigma}_{\text{cl}} \cdot F(\sqrt{s})$  with

$$F(\sqrt{s}) = \left( \frac{r_s}{r_{\text{cl}}} \right)^2 \Big|_{M_{\text{phys}} = \sqrt{s}}, \quad (6.4)$$

see Fig. 9. We conclude that the RG improved production cross section is reduced with respect to the semi-classical one, already in the regime where the semi-classical approximation is applicable, see Fig. 9. The quantitative impact of these effects on mini-black holes production at colliders, eg. the LHC, is evaluated in [18].

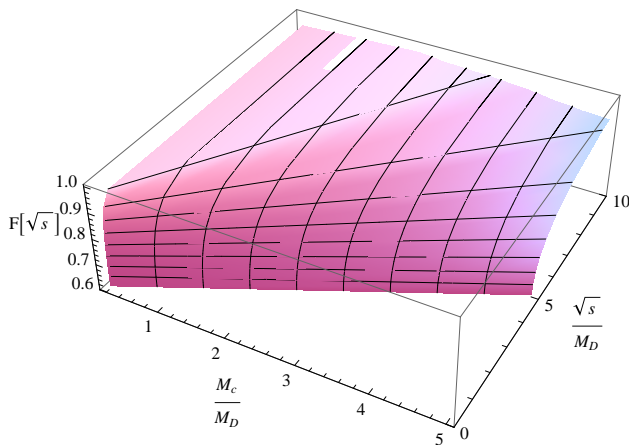


Figure 9: The gravitational form factor  $F(\sqrt{s})$  with parameter  $\gamma = \gamma_{\text{AS}}$  with  $n = 4$  extra dimensions.

### C. Trans-Planckian region

Next, we implement our RG improvement directly on the level of the classical Schwarzschild radius rather than on the level of the underlying black hole metric. To that end, we interpret the energy dependence of the form factor in the production cross section as originating from an effective energy dependence of Newton’s coupling. The latter enters the classical event horizon as

$$r_{\text{cl}}(\sqrt{s}) = \frac{1}{\sqrt{\pi}} \left( \frac{8\Gamma(\frac{d-1}{2})}{d-2} \right)^{\frac{1}{d-3}} (G_N \sqrt{s})^{\frac{1}{d-3}} \quad (6.5)$$

where the substitution  $M_{\text{phys}} = \sqrt{s}$  has already been executed. Under the assumption that the functional dependence of (6.5) on the gravitational coupling  $G_N$  remains unchanged once quantum corrections are taken into account, we can interpret the non-trivial energy-dependence of  $r_s(\sqrt{s})$  to originate from (6.5) via the energy-dependence of Newton’s coupling. Substituting  $G_N \leftrightarrow G(\sqrt{s})$ , we find

$$G(\sqrt{s}) = G_N [F(\sqrt{s})]^{\frac{d-3}{2}}. \quad (6.6)$$

Using the non-perturbative form factor  $F(\sqrt{s})$ , we conclude that  $G(\sqrt{s})$  displays a threshold behaviour, starting off at the black hole formation threshold  $\sqrt{s} \approx M_c$ , and increasing asymptotically towards  $G_N$  with increasing  $\sqrt{s}$ . Trans-Planckian scattering in gravity becomes classical:  $G(\sqrt{s})$  approaches  $G_N$  with increasing center-of-mass energy  $\sqrt{s} \gg M_D$  and the production cross section reduces to the geometrical one. This is a consequence of quantum corrections being suppressed for large black hole mass, see Sec. IV D, and thus for large  $\sqrt{s}$ .

With these results at hand, we can now turn the argument around and identify the matching  $k = k(\sqrt{s})$  which

reproduces (6.6) from the renormalisation group running of  $G(k)$ . To leading order in  $M_D/\sqrt{s} \ll 1$ , the matching

$$G_N \rightarrow G(k) \quad \text{with} \quad k \propto M_D \left( \frac{M_D}{\sqrt{s}} \right)^{1/(d-3)} \quad (6.7)$$

in (6.5) — together with  $G(k)$  from the renormalisation group, see Sec. III C — reproduces the form factor (6.4) and the semi-classical limit. The result (6.7) highlights a duality between the regime of large center-of-mass energy  $\sqrt{s}/M_D \gg 1$  of a gravitational scattering process, and the low-momentum behaviour  $(k/M_D)^{d-3} \propto M_D/\sqrt{s} \ll 1$  of the running coupling  $G(k)$  in the ‘gravitational bound state’ of a black hole.

It would be interesting to have access to the behaviour of  $G(\sqrt{s})$  at below-threshold energies, where the energy dependence of Newton’s coupling should be obtained from standard field theory amplitudes for  $s$ -channel scattering in asymptotically safe gravity [25], which become strongly dominated by multi-graviton exchange at Planckian energies [65]. For recent developments along these lines within quantum string-gravity, see [66, 67].

### D. Semi-classical limit

It is useful to compare our results with a related renormalisation group study, where qualitatively different conclusions have been reached [68]. There, black hole production cross sections are estimated from (6.5) using the RG matching

$$G_N \rightarrow G(k) \quad \text{with} \quad k \propto \sqrt{s} \quad (6.8)$$

for Newton’s coupling, with  $G(k)$  taken from the renormalisation group and  $k$  identified with  $\sqrt{s}$ , following [26]. This would be applicable if  $\sqrt{s}$  is the sole mass scale in the problem, and if  $G_N$  in (6.5) is sensitive to the momentum transfer in the  $s$ -channel. However, the matching (6.8) is in marked contrast to (6.7). Most importantly, with (6.8) no semi-classical limit is achieved in the trans-Planckian regime, because  $G(\sqrt{s})/G_N \ll 1$  becomes strongly suppressed. This conclusion is at variance with the findings of the present paper.

The origin for this difference is traced back to the following observation: the RG improved Schwarzschild radius depends on several mass scales, the Planck scale  $M_D$ , the black hole mass  $M$  and, implicitly, the momentum scale  $k$ . Identifying both the mass  $M = \sqrt{s}$  and the renormalisation group scale  $k = \sqrt{s}$  with the center-of-mass energy in a gravitational scattering process entangles mass dependences with RG scale running. In turn, the détour taken in Sec. VI C disentangles these effects by taking into account that the physics involves several mass scales. This also explains why  $M_D$  enters the matching

(6.7), besides  $\sqrt{s}$ , which is responsible for the qualitative difference with respect to (6.8).

We conclude that the set-up laid out in this work is necessary to capture the semi-classical limit of trans-Planckian scattering.

## VII. DISCUSSION

How does quantum gravity modify the physics of black holes? We have implemented quantum corrections on the level of black hole metrics, replacing Newton's constant by a coupling which runs under the renormalisation group equations for gravity.

If Newton's coupling weakens sufficiently fast towards shorter distances, it implies the existence of a smallest black hole of mass  $M_c$ . This is the case for all dimensions  $d \geq 4$  provided quantum gravity is asymptotically safe. The mass scale  $M_c$  is dynamically generated and of the order of the fundamental Planck scale  $M_D$ . Interestingly, a mere weakening of the gravitational coupling would not be enough to disallow the formation of an event horizon.

The mechanism responsible for a lower bound on black hole mass relates with the RG scaling of the gravitational coupling at the cross-over from perturbative to non-perturbative running. In consequence, the underlying fixed point is not primarily responsible for the existence of the lower bound and alternative UV completions may display a similar weakening down to length scales of the order of the Planck length.

In the semi-classical regime  $M_D/M \ll 1$ , corrections to the event horizon and black hole thermodynamics remain perturbatively small, but effects become quantitatively more pronounced with decreasing black hole mass  $M$ . Once  $M_D/M$  becomes of order one, quantum corrections are more substantial. The specific heat changes sign, the

black hole temperature displays a maximum, and vanishes with  $M \rightarrow M_c$ . This supports the view that critical black holes constitute cold, Planck-size, remnants.

Direct implications of fixed point scaling are visible in the short distance limit  $rM_D \ll 1$ . This limit becomes time-like rather than space-like as in classical Schwarzschild black holes. Also, asymptotically safe black holes with  $M > M_c$  always also display a Cauchy horizon besides the event horizon. It is noteworthy that the classical curvature singularity at the origin is significantly softened because of the fixed point, and either disappears completely, or becomes vastly reduced. The conformal structure of quantum black holes is very similar to classical Reissner-Nordström black holes, including the near horizon geometry of critical black holes which is of the  $\text{AdS}_2 \times \text{S}^{d-2}$  type.

Our results have direct implications for the collider phenomenology of low-scale gravity models. Interestingly, quantum corrections increase the domain of validity for a semiclassical description. At low center-of-mass energies, a threshold for black hole production is identified. At larger energies, quantum corrections to production cross sections lead to a new form factor. It reduces the cross section, and reproduces the semi-classical result in the trans-Planckian limit. A quantitative implementation of this scenario for mini-black hole production is given elsewhere [18]. It would be very interesting to complement this picture by explicit computations based on multi-graviton exchange at Planckian energies along the lines laid out in [25].

*Note added.*— After completion of this work, we have been informed by B. Koch that some of our results [17, 18] have been confirmed in the preprint [69].

- 
- [1] K. Schwarzschild, Über das Gravitationsfeld eines Massenpunktes nach der Einsteinschen Theorie. Sitzungsber. Preuss. Akad. D. Wiss. (1916) 189-196.
- [2] R. Emparan and H. S. Reall. Black Holes in Higher Dimensions. Living Rev. Rel. **11** (2008) 6, 0801.3471 [hep-th].
- [3] N. Arkani-Hamed, S. Dimopoulos and G. R. Dvali. The hierarchy problem and new dimensions at a millimeter. Phys. Lett. B **429** (1998) 263 [hep-ph/9803315]; I. Antoniadis, N. Arkani-Hamed, S. Dimopoulos and G. R. Dvali. New dimensions at a millimeter to a Fermi and superstrings at a TeV. Phys. Lett. B **436** (1998) 257 [hep-ph/9804398].
- [4] L. Randall and R. Sundrum. A large mass hierarchy from a small extra dimension. Phys. Rev. Lett. **83** (1999) 3370 [hep-ph/9905221]; An alternative to compactification. Phys. Rev. Lett. **83** (1999) 4690 [hep-th/9906064].
- [5] G. F. Giudice, R. Rattazzi and J. D. Wells. Quantum gravity and extra dimensions at high-energy colliders. Nucl. Phys. B **544** (1999) 3 [hep-ph/9811291].
- [6] S. Dimopoulos and G. L. Landsberg. Black holes at the LHC. Phys. Rev. Lett. **87** (2001) 161602 [hep-ph/0106295].
- [7] S. B. Giddings and S. D. Thomas. High energy colliders as black hole factories: The end of short distance physics. Phys. Rev. D **65** (2002) 056010 [hep-ph/0106219].
- [8] T. Banks and W. Fischler. A model for high energy scattering in quantum gravity. hep-th/9906038.
- [9] S. D. H. Hsu. Quantum production of black holes. Phys. Lett. B **555** (2003) 92 [hep-ph/0203154].
- [10] P. Kanti. Black holes in theories with large extra dimensions: A Review. Int. J. Mod. Phys. A **19** (2004)

- 4899 [hep-ph/0402168]. B. Webber. Black holes at accelerators. hep-ph/0511128. S. B. Giddings. High-energy black hole production. AIP Conf. Proc. **957** (2007) 69 [0709.1107 [hep-ph]].
- [11] S. Weinberg. Ultraviolet Divergences In Quantum Theories Of Gravitation. In General Relativity: An Einstein centenary survey. Eds. S. W. Hawking and W. Israel, Cambridge University Press (1979), p. 790; Living with Infinities. 0903.0568 [hep-th]; Effective Field Theory, Past and Future. 0908.1964 [hep-th]; Asymptotically Safe Inflation. 0911.3165 [hep-th].
- [12] D. F. Litim. On fixed points of quantum gravity. AIP Conf. Proc. **841** (2006) 322. [hep-th/0606044].
- [13] M. Niedermaier. The asymptotic safety scenario in quantum gravity: An introduction. Class. Quant. Grav. **24** (2007) R171 [gr-qc/0610018].
- [14] M. Niedermaier and M. Reuter, The Asymptotic Safety Scenario in Quantum Gravity. Living Rev. Rel. **9** (2006) 5.
- [15] R. Percacci. Asymptotic Safety. 0709.3851 [hep-th].
- [16] D. F. Litim. Fixed Points of Quantum Gravity and the Renormalisation Group. PoS **QG-Ph** (2008) 024, 0810.3675 [hep-th].
- [17] K. Falls, D.F. Litim, A. Raghuraman, poster presented at ERG 2008, Heidelberg (Jun 2008); K. Falls, MSc thesis, U Sussex (Aug 2008); A. Raghuraman, MSc thesis, U Sussex (Aug 2008).
- [18] D.F. Litim. Quantum gravity at the LHC, presented at Pascos 2009, DESY, Hamburg (Jul 2009) and at GDR Terascale, Heidelberg (Oct 2009); K. Falls, G. Hiller, D.F. Litim, to appear.
- [19] D. F. Litim. Fixed points of quantum gravity. Phys. Rev. Lett. **92** (2004) 201301 [hep-th/0312114]; Optimized renormalisation group flows. Phys. Rev. **D64** (2001) 105007 [hep-th/0103195].
- [20] P. Fischer and D. F. Litim. Fixed points of quantum gravity in extra dimensions. Phys. Lett. B **638** (2006) 497 [hep-th/0602203].
- [21] P. Fischer and D. F. Litim. Fixed points of quantum gravity in higher dimensions. AIP Conf. Proc. **861** (2006) 336. [hep-th/0606135].
- [22] A. Bonanno and M. Reuter. Renormalization group improved black hole spacetimes. Phys. Rev. D **62** (2000) 043008 [hep-th/0002196].
- [23] A. Bonanno and M. Reuter. Spacetime structure of an evaporating black hole in quantum gravity. Phys. Rev. D **73** (2006) 083005 [hep-th/0602159].
- [24] A. Bonanno. Astrophysical implications of the Asymptotic Safety Scenario in Quantum Gravity. PoS **CLAQG.08** (2009) 008, 0911.2727 [hep-th].
- [25] D. F. Litim and T. Plehn. Signatures of gravitational fixed points at the LHC. Phys. Rev. Lett. **100** (2008) 131301 [0707.3983 [hep-ph]]; Virtual Gravitons at the LHC. arXiv:0710.3096 [hep-ph].
- [26] J. Hewett and T. Rizzo. Collider Signals of Gravitational Fixed Points. JHEP **0712** (2007) 009 [0707.3182 [hep-ph]].
- [27] E. Gerwick and T. Plehn. Extra Dimensions and their Ultraviolet Completion. PoS **CLAQG.08** (2009) 009, [0912.2653 [hep-ph]].
- [28] F. R. Tangherlini. Schwarzschild field in  $n$  dimensions and the dimensionality of space problem. Nuovo Cim. **27** (1963) 636.
- [29] R. C. Myers and M. J. Perry. Black Holes In Higher Dimensional Space-Times. Annals Phys. **172** (1986) 304.
- [30] J. F. Donoghue. Leading quantum correction to the Newtonian potential. Phys. Rev. Lett. **72** (1994) 2996 [gr-qc/9310024].
- [31] C. P. Burgess. Quantum gravity in everyday life: General relativity as an effective field theory. Living Rev. Rel. **7** (2004) 5 [gr-qc/0311082].
- [32] H. W. Hamber and S. Liu. On The Quantum Corrections To The Newtonian Potential. Phys. Lett. B **357** (1995) 51 [hep-th/9505182].
- [33] N.E.J. Bjerrum-Bohr, J.F. Donoghue and B.R. Holstein. Quantum corrections to the Schwarzschild and Kerr metrics. Phys. Rev. D **68** (2003) 084005 [Erratum-ibid. D **71** (2005) 069904] [hep-th/0211071].
- [34] N. E. J. Bjerrum-Bohr, J. F. Donoghue and B. R. Holstein. Quantum gravitational corrections to the nonrelativistic scattering potential of two masses. Phys. Rev. D **67** (2003) 084033 [Erratum-ibid. D **71** (2005) 069903] [hep-th/0211072].
- [35] A. Akhundov and A. Shiekh. A Review of Leading Quantum Gravitational Corrections to Newtonian Gravity. Electron. J. Theor. Phys. **17** (2008) 1 [gr-qc/0611091].
- [36] M. J. Duff. Quantum corrections to the Schwarzschild solution. Phys. Rev. D **9** (1974) 1837.
- [37] D. F. Litim and J. M. Pawłowski. On gauge invariant Wilsonian flows. In *The Exact Renormalization Group*, Eds. Krasnitz et al, World Sci (1999) 168 [hep-th/9901063]; J. Berges, N. Tetradis and C. Wetterich. Non-perturbative renormalisation flow in quantum field theory and statistical physics. Phys. Rept. **363** (2002) 223 [hep-ph/0005122]; J. Polonyi. Lectures on the functional renormalization group method. Centr. Eur. Sci. J. Phys. **1** (2002) 1 [hep-th/0110026]; J. M. Pawłowski. Aspects of the functional renormalisation group. Annals Phys. **322** (2007) 2831 [hep-th/0512261]; H. Gies. Introduction to the functional RG and applications to gauge theories. hep-ph/0611146.
- [38] C. Wetterich. Exact evolution equation for the effective potential. Phys. Lett. B **301** (1993) 90.
- [39] D. F. Litim. Optimisation of the exact renormalisation group. Phys. Lett. B **486** (2000) 92 [hep-th/0005245]; Mind the Gap. Int. J. Mod. Phys. A **16** (2001) 2081 [hep-th/0104221].
- [40] K. Symanzik. Small Distance Behavior In Field Theory And Power Counting. Commun. Math. Phys. **18** (1970) 227.
- [41] M. Reuter. Nonperturbative Evolution Equation for Quantum Gravity. Phys. Rev. D **57** (1998) 971 [hep-th/9605030].
- [42] F. Freire, D. F. Litim and J. M. Pawłowski. Gauge invariance and background field formalism in the exact renormalisation group. Phys. Lett. B **495** (2000) 256 [hep-th/0009110].
- [43] D. F. Litim and J. M. Pawłowski. Renormalisation group

- flows for gauge theories in axial gauges. *JHEP* **0209** (2002) 049 [hep-th/0203005].
- [44] O. Lauscher and M. Reuter. Ultraviolet fixed point and generalized flow equation of quantum gravity. *Phys. Rev. D* **65** (2002) 025013 [hep-th/0108040].
- [45] W. Souma. Non-trivial ultraviolet fixed point in quantum gravity. *Prog. Theor. Phys.* **102** (1999) 181 [hep-th/9907027].
- [46] O. Lauscher and M. Reuter. Is quantum Einstein gravity nonperturbatively renormalizable?. *Class. Quant. Grav.* **19** (2002) 483 [hep-th/0110021]; Flow equation of quantum Einstein gravity in a higher-derivative truncation. *Phys. Rev. D* **66** (2002) 025026 [hep-th/0205062].
- [47] M. Reuter and F. Saueressig. Renormalization group flow of quantum gravity in the Einstein-Hilbert truncation. *Phys. Rev. D* **65** (2002) 065016 [hep-th/0110054].
- [48] R. Percacci and D. Perini. Constraints on matter from asymptotic safety. *Phys. Rev. D* **67** (2003) 081503 [hep-th/0207033].
- [49] R. Percacci. Asymptotic safety in gravity and sigma models. *PoS CLAQG.08* (2009) 002, 0910.4951 [hep-th].
- [50] A. Bonanno and M. Reuter. Proper time flow equation for gravity. *JHEP* **0502** (2005) 035 [hep-th/0410191].
- [51] R. Percacci. Further evidence for a gravitational fixed point. *Phys. Rev. D* **73** (2006) 041501 [hep-th/0511177].
- [52] A. Codello and R. Percacci. Fixed Points of Higher Derivative Gravity. *Phys. Rev. Lett.* **97** (2006) 221301 [hep-th/0607128].
- [53] A. Codello, R. Percacci and C. Rahmede. Ultraviolet properties of f(R)-gravity. *Int. J. Mod. Phys. A* **23** (2008) 143 [0705.1769 [hep-th]]; Investigating the Ultraviolet Properties of Gravity with a Wilsonian Renormalization Group Equation, *Annals Phys.* **324** (2009) 414 [0805.2909 [hep-th]].
- [54] C. Rahmede. Old and new results from the Wilsonian approach to gravity. *PoS CLAQG.08* (2009) 0011.
- [55] P. F. Machado and F. Saueressig. On the renormalization group flow of f(R)-gravity. *Phys. Rev. D* **77** (2008) 124045 [0712.0445 [hep-th]].
- [56] D. Benedetti, P. F. Machado and F. Saueressig. Taming perturbative divergences in asymptotically safe gravity. *Nucl. Phys. B* **824** (2010) 168 [0902.4630 [hep-th]].
- [57] M. R. Niedermaier. Gravitational Fixed Points From Perturbation Theory. *Phys. Rev. Lett.* **103** (2009) 101303; Can a nontrivial gravitational fixed point be seen in perturbation theory? *PoS CLAQG.08* (2008) 05.
- [58] H. W. Hamber. On the gravitational scaling dimensions, *Phys. Rev. D* **61** (2000) 124008 [hep-th/9912246]; H. W. Hamber and R. M. Williams. Non-perturbative gravity and the spin of the lattice graviton, *Phys. Rev. D* **70** (2004) 124007 [hep-th/0407039]; H. W. Hamber and R. M. Williams. Quantum gravity in large dimensions, *Phys. Rev. D* **73** (2006) 044031 [hep-th/0512003].
- [59] J. Ambjorn, J. Jurkiewicz and R. Loll. Emergence of a 4D world from causal quantum gravity. *Phys. Rev. Lett.* **93** (2004) 131301 [hep-th/0404156]; Spectral dimension of the universe. *Phys. Rev. Lett.* **95** (2005) 171301 [hep-th/0505113].
- [60] G. W. Gibbons and S. W. Hawking. Action Integrals And Partition Functions In Quantum Gravity. *Phys. Rev. D* **15** (1977) 2752.
- [61] S. W. Hawking in *General Relativity: an Einstein Centenary Survey*, Eds. S. W. Hawking and W. Israel (Cambridge University Press, 1979).
- [62] P. M. Stevenson. Optimized Perturbation Theory. *Phys. Rev. D* **23** (1981) 2916.
- [63] P. K. Townsend. Black holes. gr-qc/9707012.
- [64] D. M. Eardley and S. B. Giddings. Classical black hole production in high-energy collisions. *Phys. Rev. D* **66** (2002) 044011 [gr-qc/0201034].
- [65] G. 't Hooft. Graviton Dominance in Ultrahigh-Energy Scattering. *Phys. Lett. B* **198** (1987) 61.
- [66] D. Amati, M. Ciafaloni and G. Veneziano. Towards an S-matrix Description of Gravitational Collapse. *JHEP* **0802** (2008) 049 [0712.1209 [hep-th]].
- [67] G. Marchesini and E. Onofri. High energy gravitational scattering: a numerical study. *JHEP* **0806** (2008) 104 [0803.0250 [hep-th]].
- [68] B. Koch. Renormalization group and black hole production in large extra dimensions. *Phys. Lett. B* **663** (2008) 334 [0707.4644 [hep-ph]].
- [69] T. Burschil and B. Koch. Renormalization group improved black hole space-time in large extra dimensions. 0912.4517 [hep-ph].